†Current address: Instituto Oceanográfico, Universidade de São Paulo, Praça do Oceanográfico 191, 05508-120 São Paulo, SP, Brazil; scardia@usp.br.

GSA Bulletin; Month/Month 2014; v. 1xx; no. X/X; p. 000–000; doi: 10.1130/B30990.1; 11 figures; 3 tables.

Evidence for late Alpine tectonics in the Lake Garda area (northern Italy) and seismogenic implications

Giancarlo Scardia[1,†], Andrea Festa[2], Giovanni Monegato[3], Roberta Pini[4], Sergio Rogledi[5], Fabrizio Tremolada[6], and Fabrizio Galadini[7]

[1]Istituto di Geologia Ambientale e Geoingegneria, CNR, via Salaria km 29.300, I-00016 Monterotondo Scalo (Roma), Italy

[2]Dipartimento di Scienze della Terra, Università di Torino, Via Valperga Caluso 35, I-10125 Torino, Italy

[3]Istituto di Geoscienze e Georisorse, CNR, via Valperga Caluso 35, I-10123 Torino, Italy

[4]Istituto per la Dinamica dei Processi Ambientali, CNR, Piazza della Scienza 1, I-20126 Milano, Italy

[5]ENI E&P, via Emilia 1, I-20097 San Donato Milanese, Italy

[6]RPS Energy, Goldsworth House, Denton Way, Goldsworth Park, GU213LG Woking, UK

[7]Istituto Nazionale di Geofisica e Vulcanologia, via di Vigna Murata 605, I-00143 Roma, Italy

ABSTRACT

We investigated the recent evolution of the Po Plain–Alps system by integrating subsurface geophysical data from the Po Plain with new stratigraphic and structural observations from the

southern Alps margin. Inversion of structural data and chronology provided by stratigraphic constraints led to the definition of three tectonic events since the Pliocene, namely, the intra-Zanclean, the Gelasian, and the middle Pleistocene, driven by an axis of maximum compression formerly oriented NE (intra-Zanclean) and then to the NNW (Gelasian and middle Pleistocene). The associated deformation has been accommodated by two sets of faults consisting of NNE-trending thrust faults, mostly represented in the western sector of Lake Garda, and NW-trending strike-slip faults, observed in the southern and eastern sectors. The interplay between these two sets of faults is interpreted to produce short (<10 km length) thrust ramps activated in left transpression, bounded by longer (30–60 km) transfer faults activated in a right-lateral strike-slip motion. Based on this structural model, we infer moderate seismicity ($M_w < 6$) associated with the NNE-directed thrusts and stronger earthquakes (also $M_w > 6.5$) along the NW-trending strike-slip faults. In this framework, the newly defined Nogara fault and the Sant'Ambrogio fault, all pertaining to the NW-trending system, are regarded as potential candidates for the seismogenic source of the January A.D. 1117 event, the most destructive earthquake in the Po Plain.

INTRODUCTION

After a complex succession of deformation phases, the traditional geologic view constrains the end of Alpine tectonics in the Po Plain to the late Messinian (Pieri and Groppi, 1981; Castellarin et al., 1992; Fantoni et al., 2004), with residual activity confined in the eastern southern Alps (e.g., Castellarin and Cantelli, 2000; Galadini et al., 2005). This view mainly relies on the occurrence of postorogenic Pliocene marine deposits sealing the folded and eroded Mesozoic–Cenozoic Alpine bedrock (Castellarin et al., 1992). However, geomorphologic, seismological, and geodetic evidence (e.g., Desio, 1965; Anderson and Jackson, 1987; D'Agostino et al., 2008; Livio et al., 2009) clearly points to a still ongoing deformation in the southern Alps and Po Plain, the study of which is the aim of the present work.

Increasing scientific sensibility of the seismic hazard of the Po Plain has led to modern studies based on punctual paleoseismological investigations (Galadini and Galli, 1999; Galadini et

al., 2001; Livio et al., 2009). Moving from these studies, our present work aims to depict a new structural model for the Po Plain that accounts for the largely ignored Pliocene–Pleistocene tectonics of the southern Alps and seismogenic implications at regional scale. A special emphasis is given to the Lake Garda area because of (1) its complexity as an interference area between two different structural styles, (2) the occurrence of deformed Pliocene–Pleistocene deposits, and (3) the occurrence of damaging historical earthquakes (e.g., A.D. 1117, M_w 6.7; A.D. 1222, M_w 5.8; A.D. 1891, M_w 5.9; A.D. 1901, M_w 5.5; Locati et al., 2011; Pessina et al., 2013). We based our study on the integration of subsurface geophysical data with new direct stratigraphic and structural observations, gathered by means of detailed geological survey along the southern Alps margin. Taking into account that sedimentation (in the Po Plain) or erosion (in the Alps) rates are much higher than the tectonic strain rate (e.g., Livio et al., 2009; Burrato et al., 2012), we focused on Pliocene and early Pleistocene deposits, where the cumulative deformation is expected to be more evident in the stratigraphic record.

REGIONAL BACKGROUND

The tectonic setting of the southern Alps has a complex history, including Mesozoic rifting and convergence between the European and Adriatic plates since the Late Cretaceous. Thrusting of the Paleozoic basement and its sedimentary cover during the Miocene represented the final, postcollisional phase of the Alpine orogeny, which resulted in the formation of a fold-and-thrust belt composed of south-verging thrust sheets (e.g., Laubscher, 1985; Picotti et al., 1995).

The Lake Garda area lies between two sectors characterized by different structural styles. To the west, the "Giudicarie belt" consists of NNE-trending, transpressive thrusts and folds (Fig. 1). The eastern sector is characterized by the rigid block of the Lessini Mountains, mainly deformed by the NW-trending, strike-slip Schio-Vicenza fault system. Since the late Messinian, Apennines-related flexural subsidence has involved the southern sector of the Alps, resulting in the southward tilting and burial of the outermost Alpine thrusts (e.g., Fantoni et al., 2004). Southward tilting also involved the former Alpine foreland, producing a regional monocline dipping ~5° toward the

Apennines (Mantova monocline; Fig. 1). During the Pliocene and the early Pleistocene—now including the Gelasian stage (Gibbard et al., 2010)—the stepwise northward migration of the Apennines produced basinwide structural modifications and the deposition of two tectono-stratigraphic groups, namely, EP (Pliocene) and LP **[[Q: Spell out EP and LP at first use here?]]** (Pleistocene), produced by the intra-Zanclean and Gelasian tectonic phases, respectively (Ghielmi et al., 2010). After the severe Pliocene tectonics, a gradual decrease in the Apennines compressional deformation occurred during the early Pleistocene, as indicated by the reduced growth of the existing structures (Ghielmi et al., 2010). A probably associated decrease in subsidence led the Po Basin to complete infilling (sequences PS1–PS3 within the LP group; Scardia et al., 2012).

In a context of low deformation rates, the climatic signal becomes evident in the stratigraphic record of the Po Plain with the formation of the R surface (base of sequence PS2), a regional seismic horizon that marks the onset of the major Pleistocene glaciations at ca. 0.9 Ma (Muttoni et al., 2003). Since the middle Pleistocene, the outward migration of the Apennines seems to have stalled, and no formation of new thrusts is documented (Picotti and Pazzaglia, 2008). Broadly at the same time, erosion-driven isostatic rebound is inferred as the dominant process in the western southern Alps (Scardia et al., 2006, 2012). Associated decrease in accommodation space forced fluvial systems to prograde basinward, triggering the formation of the Y surface (base of PS3 sequence) at ca. 0.45 Ma (Scardia et al., 2012).

Land exposures preserve a fragmentary and marginal record of the Pliocene–Pleistocene events, making their remarkable and direct information very scattered. Sparse Pliocene deposits and late Cenozoic conglomerates have been known along the Alpine margin since early studies (see following section), and their revision in the present study is aimed at framing them in the aforementioned regional stratigraphic layout, with mutual advantage provided by the better chronological constraints of the outcrops and the stratigraphic continuity of the subsurface stratigraphy.

SUBSURFACE GEOLOGY

The subsurface geologic structure of the Po Plain was depicted in the early 1980s by Pieri and Groppi (1981). A recent reappraisal summarized in Fantoni et al. (2004) mainly dealt with the western and central sectors of the buried southern Alps front. Moving from these studies, we reinterpreted the whole ENI **[[Q: Please spell out ENI at first use.]]** seismic data set of the central and eastern Po Plain, focusing on the largely ignored Mantova monocline. Following the approach of Fantoni et al. (2004), we mapped the main buried structural features at different stratigraphic levels, projecting onto the horizontal plane the hanging-wall cutoffs at the Aptian-Albian unconformity (top of the Mesozoic calcareous rocks) and at the youngest horizon (Messinian to early Pliocene) of the Cenozoic terrigenous units. Some differences in details between the structures mapped in Figure 1 and those from previous studies are ascribable to a different interpretation of seismic data and to the application of slightly different models of structural style.

Southern Alps Structures

The northern sector of the Po Plain is characterized by the occurrence of the southern Alps buried fronts, which interact in their outermost portion with the Apennines fronts. Interaction takes place along a deeper, E-W–oriented structure (the Corneliano-Bordolano axis; Fig. 1), representing a residual foreland located between the southern Alps and the Apennines thrusts. The southern Alps are characterized by two different structural styles. Between Lake Como and Lake Iseo, there are imbricate, south-verging thrusts involving both the Mesozoic calcareous succession and the overlying Cenozoic terrigenous deposits. The metamorphic basement seems to be clearly involved only northward of the Franciacorta and Brescia faults (Fantoni et al., 2004; Fig. 1), where low-angle detachment planes can be observed at relatively shallow depth.

South of Lake Iseo, the southern Alps structures experience abrupt rotations or interruptions (Fig. 1). This behavior is attributed to an inherited, deeper, NNE-trending fault rooted in the basement (Iseo fault; see also section 12 of Pieri and Groppi [1981] and Figure 7a of Fantoni and Franciosi [2010]). The Iseo fault corresponds to a major extensional fault of Mesozoic or Permian age, already inferred in literature from land exposures (i.e., Lake Iseo–Oglio River line [Castellarin

et al., 1992], Sebino faults [Bertotti et al., 1993], Val Camonica line [Cassinis and Perotti, 1996]). East of this fault, the southern Alps south-verging thrusts in Cenozoic terrigenous units shift to one (Fantoni et al., 2004) or two major, north-verging back thrusts (Livio et al., 2009), reflecting a different arrangement of the deeper structures and, ultimately, a paleogeographic conditioning (see also Ravaglia et al., 2006).

More eastward in the Lake Garda area, the Alpine thrusts evolve in lateral ramps according to a NNE-trend (Fig. 1). Here, decreasing offset in the outermost structures records the transition to the foreland, where incipient, high-angle faults show a slight inversion of the movement with respect to their former Mesozoic extensional behavior (Solferino fault; Figs. 1 and 2A). For the NE-trending Sirmione fault, interpretation of the available seismic lines shows a vertical offset of ~2 km (~1 s two-way traveltime at ~4 km/s; Fig. 2A). This fault is correlative with the inferred structure known in literature as the Sirmione-Garda fault (Carton and Castaldini, 1985, and references therein). Pliocene–Pleistocene seismic reflectors in the Lake Garda area are poorly imaged in the available seismic profiles, but some disturbance along the Sirmione fault seems to occur up to the level of the R surface (base of the PS2, ca. 0.9 Ma; Fig. 2A), with the western sector uplifted with regards to the eastern sector.

On the whole, abrupt changes in strikes and dips of faults at shallow depths suggest a control exerted by lineaments predating the Alpine compressional phases. These older faults may be reactivated or have controlled the trajectory of newly formed faults. The structural elements controlling this behavior are Mesozoic extensional and transfer faults, often reactivated as lateral ramps of the new Alpine thrusts or accommodating the flexural tilting in the foreland sector. We also observed that thrusts in Cenozoic terrigenous units often develop frontal ramps in correspondence with the structural steps provided by the underlying Mesozoic normal faults (e.g., Piadena fault; Fig. 1; see also Picotti et al., 2007).

Foreland Structures

The present-day foreland is represented by the Mantova monocline, a regional, south-dipping structure that lies between the Alpine and Apennines fronts (Figs. 1 and 2B). Interruptions and offsets in Mesozoic reflectors point to the occurrence of blocks bounded by subvertical faults, as observed in the Lessini Mountains exposures. The main structural setting consists of NW-oriented extensional faults, bounding tilted blocks of variable size and sometimes interrupted by transfer faults (Figs. 1 and 2B). All over the Mantova monocline, relatively lifted and lowered blocks can be recognized in the Mesozoic succession. The lowered blocks identify more subsiding troughs like the Suzzara Basin, bounded eastward by the NW-trending Viadana fault and interrupted northward by the NE-trending Mantova fault (Fig. 1).

Among the NW-trending faults, the Nogara fault (Figs. 1 and 2B) appears to be the most notable. It consists of a subvertical plane that bears variable displacements, often showing reversal of the downthrown and upthrown sides. This feature suggests a scissor fault behavior, characterized by a strike-slip deformation mechanism. The evidence of this fault is not always well traceable in the ENI seismic data set, probably because the seismic resolution is ~20–30 m, and it does not allow relatively smaller offsets to be detected. The estimated length of this fault is ~60 km, and in the best two-dimensional (2-D) seismic profile, deformation or interruption of seismic reflectors seems to occur at least up to the Y surface (Fig. 2B).

GEOLOGY OF LAND EXPOSURES

Geological survey was carried out on Pliocene and early Pleistocene deposits of the Lake Garda area, with the aim of detecting evidence of faulting and constraining the age of deformation. We chose relatively older deposits with respect to the common practice in active tectonics studies (e.g., Galadini et al., 2012), because in an area where glacial erosion has been the main shaping process (with rates much higher than those related to the tectonic activity), only the few sparse remains of Pliocene–Pleistocene deposits may provide evidence of strain by accumulated deformation.

We present data from three sites distributed in the western side, eastern side, and the middle of the Lake Garda area, respectively (Fig. 1). These sites bear evidence of the different structural styles:

(1) The western sector is mainly characterized by NNE-directed, SE-verging thrust faults belonging to the Giudicarie belt.

(2) The eastern sector, corresponding to Lessini Mountains, consists of rigid blocks bounded by subvertical, NW/NNW strike-slip faults (Schio-Vicenza fault system).

(3) The central sector records the complex structural interference between the differently oriented fault systems, described herein, as observed northward in the Trento area.

These structural styles are reflected in the seismotectonic settings of the Lake Garda area, where focal plane solutions document dominant contractional and strike-slip components in the Giudicarie belt and in the Lessini Mountains area, respectively (Viganò et al., 2008).

For chronostratigraphic considerations, we refer to the Lourens et al. (2005) time scale, modified after Gibbard et al. (2010) and Backman et al. (2012).

Western Sector

Stratigraphy

The area south of Brescia is characterized by the occurrence of isolated reliefs, which are related to the growth of buried thrusts since at least the middle Pleistocene (Desio, 1965). Moving along the eastern bank of Chiese River, Pliocene and early Pleistocene deposits are exposed in few and sparse outcrops (Cremaschi, 1987), where no significant deformation has been observed. The most striking evidence of late Alpine tectonics is found in the western bank of Lake Garda at San Bartolomeo Hill, where Pliocene marine deposits have been uplifted to an elevation of ~500 m above sea level.

The San Bartolomeo Hill Formation (Baroni et al., 1995) consists of a transgressive-regressive cycle subdivided in three members, named SB1, SB2, and SB3 from bottom to top, respectively (Fig. 3). SB1 and SB3 display very similar lithology and petrography and can be

205 separated with confidence only when the intermediate SB2 member occurs. The SB1 member may
206 reach a maximum thickness of ~170 m and consists of coarse-grained, massive to crudely bedded
207 conglomerate, unconformably lying on the bedrock (Fig. 3). The conglomerate passes upward to
208 50-m-thick, massive to laminated, fossiliferous silty clays (SB2). Toward the top, sand and gravel
209 lenses are common, as well as intervals with a very thin lamination and organic-rich layers. The
210 succession is sealed by an ~25-m-thick conglomerate (SB3), with roughly the same petrography
211 composition as the underlying gravels. The boundary between the fine-grained deposits and the
212 upper conglomerates is erosional. The latter sediments show an increasing organization toward the
213 top, from crudely bedded and coarse grained to horizontal or planar cross-bedded and medium to
214 fine grained.
215 Clast petrography of SB1 is dominated by dolostone fragments (57%), with the overall
216 carbonates exceeding 80%; this composition points to a local drainage from the southern Alps
217 sedimentary cover (Fig. 4), also suggested by the ~50-cm-sized blocks of marly limestone
218 ("Scaglia" facies) observed at the base. The SB2 and SB3 members show a progressive enrichment
219 in volcanic (>10%) and metamorphic clasts (~5%), interpreted as a mixture of the local drainage
220 with the wider Adige catchment (Table 1; Fig. 4).
221 Based on facies analysis, the lower conglomerate SB1 is interpreted as an alluvial fan. Even
222 if the boundary between this latter and the upper SB2 member is not observed, we interpret the
223 fining-upward trend of SB1 coupled with the occurrence of marine clays at the top (SB2) as a
224 unique transgressive event. The coarsening upward at the top of SB2 and the very thin laminated
225 organic-rich layers point to a gradual shallowing of the environment, from shelf to lagoon settings.
226 Braid-plain deposits of SB3 close the regressive sequence.
227 We performed calcareous nannofossil investigations on 12 samples collected in the SB2
228 marine deposits (Table 2). The analyzed samples show a scarce content in nannofossils,
229 characterized by a moderate conservation and abundant reworked taxa from the Mesozoic and
230 Paleogene. All four samples collected in the northeastern sector of San Bartolomeo Hill turned out

231 to be barren and are not reported in Table 2. The presence of *Pseudoemiliania ovata*, *Sphenolithus*
232 *abies*, and *Pseudoemiliania lacunosa* allows the SB2 member to be referred to the NN14–NN15
233 zone (Martini, 1971; 4.04–3.81 Ma, late Zanclean). In addition, the first occurrence of *P. lacunosa*
234 at the top of the succession provides an age of 3.82 Ma (Backman et al., 2012).
235 Samples collected for pollen analysis in fine-grained levels of the lower SB1 conglomerate
236 turned out to be devoid of pollen. One sample collected in the SB2 marine clays (Fig. 3, sample
237 SB22) yielded limited pollen concentration (<1800 grains/cm^3 of sediment), which was sufficient to
238 provide basic paleoenvironmental and biostratigraphic information (Table 3). The pollen spectrum
239 originates from conifer forests of cool climate, dominated by *Cathaya* (37% of the identified grains)
240 accompanied by pines, spruce, and hemlock. Pollen of woody angiosperms occurs as sporadic
241 items. Precise biochronologic attribution is not possible with a single pollen spectrum, but some
242 simple considerations can be derived: (1) The abundance of *Cathaya* rules out any attribution to the
243 early Pleistocene, and (2) comparison with the available data from the Pliocene of northern Italy
244 (Bertini, 2001) may suggest that sample SB22 was deposited sometimes after 4 Ma and before 2.6
245 Ma, in good agreement with the nannofossil biostratigraphic data.
246 Based on the late Zanclean age of the whole SB2 member and its supposed continuity with
247 the underlying SB1 member in a unique transgressive event, we suggest an early Pliocene age for
248 the lower conglomerate, in agreement with Cita (1955). Our interpretation differs from the latest
249 Messinian age of Picotti et al. (1997), relying on the findings of *Melanopsis* sp. at the base of SB2.
250 A generic *Melanopsis* sample documents fresh/brackish and warm waters (Esu, 1980) but has poor
251 biostratigraphic value. In our interpretation, the occurrence of *Melanopsis* marks an early Pliocene
252 transitional environment occurring between the SB1 alluvial-fan drowning and the marine
253 ingression of the SB2 member.
254 ***Structural Geology***
255 The bedding attitude of the San Bartolomeo Hill Formation is subhorizontal, and, according
256 to previous studies, the whole succession appears to be displaced by a set of NW-trending

extensional faults characterized by small vertical offset (Venzo, 1957; Baroni et al., 1995; Picotti et al., 1997). On the basis of the structural analysis of mesoscopic deformation of pebbles, three distinct deformation events were recognized in the San Bartolomeo Hill Formation: an older contractional event with a maximum stress axis ($\sigma 1$) oriented at N45°, followed by two younger extensional phases, with minimum stress axis ($\sigma 3$) oriented at N50° and at N305°, respectively (Picotti et al., 1997). The older extensional event with minimum stress axis ($\sigma 3$) oriented at N45° is explained as being due to a forebulge tensional stress during the early Pliocene northward migration of the Apennines (Picotti et al., 1997).

Our survey did not provide new data about the normal faults reported in previous studies. Therefore, the actual contribution of the San Bartolomeo Hill to our tectonic scenario relies on age, elevation, and bedding attitude of the Pliocene deposits coupled with the structural analysis carried out by Picotti et al. (1997).

Eastern Sector

Stratigraphy

Pliocene or early Pleistocene deposits were never clearly identified in the eastern Lake Garda bank, with the exception of the Montecio Conglomerate, of generic Neogene age (Venzo, 1961). The conglomerate is exposed at Montecio, close to Sant'Ambrogio di Valpolicella, and along the Cà Verde depression (Fig. 5). It rests with an erosional lower boundary on the bedrock and develops with horizontal and planar cross-bedded, well-sorted, well-rounded, fine-grained gravels. Up section, the clast size increases to 25–30 cm, and the conglomerate is crudely bedded. The succession ends with a set of gravel-to-sand fining-upward cycles. The overall thickness is ~50 m. Pebbles are composed of limestones and dolostones with few clasts of volcanic and metamorphic rocks. Sand petrography shows abundance of quartz (30–45%), limestone (up to 34%), and phyllites (15–19%), with a common occurrence of acidic volcanic rocks (up to 11%) (Table 3). Facies associations suggest that the Montecio Conglomerate was deposited by a shallow, gravel-bed river. The good organization of the body rules out deposition by a local stream, but

rather points to deposition in a braid plain with local high-energy episodes. According to the petrographic composition, provenance of the Montecio Conglomerate can be constrained to a paleoriver draining the Mesozoic and Tertiary sedimentary cover and volcanic rocks of the east Lake Garda bank, Lessini Mountains, and a small portion of the Valsugana basement (Figs. 1 and 4).

Dating the Montecio Conglomerate at Sant'Ambrogio is a hard task due to lack of fossils and fine-grained layers suitable for pollen or paleomagnetic analyses. Northward, at Rivoli V.se **[[Q: Please spell out V.se here.]]** (Fig. 5A), we observed gravels with petrographic composition similar to the Montecio Conglomerate. The gravel deposit fills tectonic fractures in the Mesozoic bedrock, is strongly weathered, and bears a wealth of fossil microfauna, among which the late Villanyan *Mimomys pliocaenicus* (Sala et al., 1994) is ascribable to the Gelasian (2.59–1.81 Ma; Nomade et al., 2014; Bellucci et al., 2014). The petrographic correlation between the Sant'Ambrogio and Rivoli exposures points to the same paleodrainage (now completely dismembered) for both the deposits and can support their contemporaneity. The Gelasian microfauna at Rivoli is not coeval to the gravels, because the strong weathering would have destroyed the very thin bones. Therefore, the occurrence of *M. pliocaenicus* should instead be considered as penecontemporaneous to the opening of the fractures. These bones, being small, fragile, and relatively lightweight, are usually found in primary deposition as a product of nocturnal bird predation activity (e.g., owls), for which habitat shelters are in rocky and cliffs areas (e.g., Andrews, 1990) compatible with the environment of Rivoli. The *M. pliocaenicus* microfauna at Rivoli allows the Montecio Conglomerate to be referred to a pre-Gelasian time, most likely the Pliocene (see discussion in ~~section 4~~ **[[Q: Please cite section title here.]]**).

Structural Geology

The Montecio Conglomerate fills the NW-oriented Cà Verde depression and is cut by NW- to WNW-directed fault systems (Fig. 5B). The WNW fault system, which consists of high-angle right-lateral faults dipping mainly to NE, is pervasive at meso- to macroscale (Fig. 6B) and is

bounded by the NW-directed one. At the mesoscale, the faults show a right-stepping en echelon arrangement with meters- to tens-of-meters-wide overlapping zones. Close to the faults, pebble surfaces are polished and locally contain rounded-to elongated solution pits and striae formed by the impact of differently sized pebbles (Fig. 6A). In general, the solution pits occur on opposite poles of the pebble surfaces according to the orientation of the maximum compressional stress parallel to their long axis (Caputo et al., 2010, and references therein). Striae and grooves on pebble surfaces vary from parallel to curved on flat surfaces. Grooves are commonly millimeters to centimeters long and 0.1–0.2 mm wide, and striae are 4–5 cm long (Fig. 6A). The direction of both striae and grooves on pitted pebbles is well consistent with that of slickenlines measured on NW faults. Paleostress analysis attempted with the few available data indicates a NNW-SSE orientation (~N175°) of the maximum compressive axis of stress ($\sigma 1$) (Fig. 5C).

Meter-scale, right-lateral faults with E-W direction also locally occur. The most notable example is a high-angle, north-dipping fault consisting of two main surfaces that bound a 50-cm-thick fault breccia (Fig. 6C). Extensional slickenlines occur on the fault surface, representing the reactivation of prevalent right-lateral movements, as indicated by S-C shears within the fault breccia.

In addition to the Sant'Ambrogio area, gravels ascribable to the Montecio Conglomerate fill NE open fractures in the Rivoli V.se **[[Please spell out here.]]** area (Figs. 5 and 6D), which cut subvertical NNE-directed, left-lateral faults. These open fractures are interpreted, in analogy with what was observed at Sant'Ambrogio, as tensile joints produced by right stepovers of the NW-directed right-lateral fault system.

Central Sector

Stratigraphy

The central sector is largely occupied by Lake Garda and by middle to late Pleistocene glacial deposits (Cremaschi, 1987). Thankfully, the Sirmione peninsula (Fig. 7) is located in the middle of Lake Garda, bearing Late Cretaceous calcareous bedrock (Cita, 1949) and a conglomerate

of uncertain age (Sirmione Conglomerate; Venzo, 1965). The Sirmione Conglomerate is widely exposed along the eastern bank of the Villa Cortine hillock, where it unconformably lies on late Campanian cherty and marly limestones (nannofossil zone CC22c of Sissingh, 1977; Table 2). The Sirmione Conglomerate has been attributed to the late Miocene (Venzo, 1965) as well as to the middle Pleistocene (Cremaschi, 1987), and it is distinguished in two members by facies and sediment composition (Fig. 8). The lower member SIR1 is 11–13 m thick (lower boundary not observed) and consists of massive, coarse-grained, matrix-supported gravel, with boulders from angular (limestones) to rounded (porphyries) shape, passing upward to a crudely bedded conglomerate, sealed by a massive fine-grained layer, with sandstone lenses and lateral continuity of several tens of meters. The transition to the upper member SIR2 is gradual and characterized by a 5–6-m-thick interval of crudely bedded, clast-supported conglomerate, showing a better sorting, rounded clasts, and a remarkable minor amount of porphyries. Facies association points to proximal braid-plain environment characterized by longitudinal bars and thick debris-flow deposits with boulders and blocks up to 1 m size, passing upward to a shallow, gravel-bed river braid plain (Miall, 2006). The SIR2 member is composed of horizontal to planar, cross-bedded conglomerate, showing well-sorted and clast-supported character; pebbles are dominated by limestone and chert. Laminated to massive sandstone lenses occur more frequently toward the top. Very rare and thin fine-grained layers were observed at the top of sandstone lenses. The dominant horizontal and planar cross-bedded gravel facies association is interpreted as a vertical stack of shallow, gravel-bed river channels, pointing to a braid-plain depositional system. The average thickness is 12–15 m, but in the northernmost outcrops, the SIR2 member lies directly on the bedrock. Samples collected for pollen analysis in the fine-grained levels were barren.

Sand petrography of the two members shows a clearly different provenance (Table 1; Fig. 4). SIR1 is polygenic, with a dominance of dolostone fragments (>45%), common limestone (~15%), acidic volcanic (~10%), and metamorphic fragments (~9%). The gradual transition to the upper member shows an increase in limestone grains. Limestones become dominant in the SIR2

member (>48%), coupled with cherts (>10%); dolostones are still abundant (~30%), while the other parameters are poorly represented. Comparison with source areas and available databases (Gazzi et al., 1973; Garzanti et al., 2006; Monegato et al., 2010; Garzanti et al., 2011) points to an Adige catchment provenance for SIR1, as also assessed by the occurrence of granodiorites and gneiss characteristic of the Bressanone area (northeastern sector of the Adige catchment). The SIR2 provenance is conversely related to a smaller drainage, likely located eastward of the present Lake Garda in the Mesozoic sedimentary cover of the southern Alps.

Paleoenvironmental and chronologic constraints were obtained by means of pollen and paleomagnetic analyses on the fine-grained layer from the SIR1 member (Fig. 8). Three pollen spectra display a lack of floral elements (e.g., *Tsuga*, *Carya*, *Pterocarya*; Table 3) widely distributed on the southern Alps margin during the preglacial early Pleistocene (Ravazzi and Rossignol Strick, 1995; Muttoni et al., 2007). Taxa occurring in these samples derived indeed from open conifer forests and steppic scrublands peculiar of the cold and dry climatic conditions that typified Pleistocene major glacial stages (Muttoni et al., 2003). Samples also yielded an abundance of reworked palynomorphs of Pliocene and older time intervals, suggesting a strong erosional input from older terrains. Paleomagnetic analyses on 12 samples show the existence of a low to medium unblocking temperature component, partially or, more frequently, totally superimposed on a high unblocking temperature. The lower unblocking temperature component, removed between room temperature and less than ~600 °C, bears northerly down-pointing inclinations and is regarded as a recent magnetization overprint. The characteristic component, when resolved, is removed to the origin of the demagnetization axes in the temperature range between ~500 °C and ~680 °C and bears a reverse magnetization regarded to be acquired at sediment deposition (DRM). The pervasive normal polarity overprint cannot be interpreted as thermoviscous because the organic matter (i.e., pollen) should have been erased by heat. Therefore, new formation of magnetic mineral (sulfides and magnetite) during the normal polarity Brunhes chron (<0.78 Ma) is the most likely cause for the normal polarity overprint, thus interpreted as chemical **[[or characteristic?]]** remanent

magnetization (CRM). The site mean value, calculated by integrating the analysis of remagnetization circles and the few retrieved paleomagnetic directions (McFadden and McElhinny, 1988), provided declination = 215° and inclination = –68°.

On the whole, taking into account the pollen results and the paleomagnetic data, the SIR1 member of the Sirmione Conglomerate can be ascribed to a glacial stage of the reverse polarity late Matuyama chron (0.99–0.78 Ma; Muttoni et al., 2003, 2007; Scardia et al., 2010).

Structural Geology

Two main fault systems, NW- and NNE-directed, respectively, occur in the Sirmione peninsula. A NNE fault displaces the Sirmione Conglomerate along the eastern bank of the peninsula (Fig. 7). It is composed of two main high-angle fault zones, decimeters to meters wide and tens to hundreds of meters long, each of which consists of several-meters-long anastomosed faults with overlapping to overstepping relationships in outcrop (Figs. 9A and 9B). Striated calcite fibers drape the fault surfaces, indicating left-lateral movement. Secondary extensional components also occur. Within the overlapping fault segments, pebbles are locally reoriented and aligned parallel to the faults. Dragging pebbles also occur in the fault's hanging wall. The same fault system also displaces the Late Cretaceous bedrock. Not-mappable left-lateral faults can be observed in the northern part of the Sirmione peninsula (the "Grotte di Catullo" area; Fig. 7), where they show tens-of-meters-long surfaces with positive flower structures in outcrop. Locally, the superposition of striated calcite fibers indicates extensional reactivation of the left-lateral movements.

The second fault system, NW-directed, was observed only in the Late Cretaceous succession (Fig. 7), and it mainly consists of NE-dipping, right-lateral faults with a secondary reverse component of movement. In the northern termination of the Sirmione peninsula, this fault system consists of two main en echelon right-stepping faults, hundreds of meters long, which are connected by tens-of-meters-long N faults (Fig. 7). The main NW fault segment shows horsetail termination at its western tip, displacing with right-lateral movement the NE left-lateral fault observed in the bedrock of the Grotte di Catullo area (Figs. 9C and 9D). The architecture of the NW fault system

strongly resembles that described in the eastern sector in the Sant'Ambrogio area (see ~~section 3.2.2~~ **[[Please cite section title here.]]**). On the whole, all the observed faults and fractures are consistent with σ1 oriented according to a NNW-SSE direction (~N172°) (Fig. 7).

DISCUSSION

By integrating stratigraphic and structural data from land exposures with evidence from subsurface geology, we interpret a succession of tectonic events recorded along the southern Alps margin in the Lake Garda area since the Pliocene (Fig. 10).

In the western sector, we recognize and constrain the following deformation phases:

(1) Late Zanclean subsidence and marine transgression: In our interpretation, this event is materialized by the SB1 deposition and the SB2 marine transgression. It can be considered coeval to a regional stratigraphic event recognized all along the southern Alps margin and biostratigraphically constrained to the early Pliocene (Raffi and Rio, 1978; Favero and Grandesso, 1982; Brambilla and Lualdi, 1986). At this time, the sea penetrated deeply into the Alpine valleys producing a *costa a rias* morphology (Corselli et al., 1985). This regional event can be referred to the intra-Zanclean tectonic phase of Ghielmi et al. (2010), when the northward migration of the Apennine fronts flexed the Alpine orogen, triggering subsidence along the southern Alps margin and marine transgression into the Alpine valleys. Our biostratigraphic data allow for firmly constraining this tectonic event to the late Zanclean at around the NN14–NN15 nannofossil biozones (4.04–3.81 Ma).

(2) Uplift of the San Bartolomeo Hill: The San Bartolomeo Hill Formation ends with a regressive sequence where braid-plain deposits prograde into a coastal/lagoon environment in the latest Zanclean. Somewhere in time since that moment forward, i.e., since the Piacenzian, the deposits were uplifted to an elevation of ~500 m, providing an uplift rate of 0.13 mm/yr. This long-term value is a minimum value, as uplift likely started after the deposition of SB3, and it may average a complex history consisting of more than one phase of uplift and periods of tectonic quiescence over a time interval of ~4 m.y. The uplift was initially produced by a N45° horizontal

σ1, which can testify to an Apennine-driven compressive stress field (Picotti et al., 1997). The two youngest deformations bear vertical σ1 and horizontal σ3, which rotates from N50° to N305°. The first N50° extensional deformation event is broadly coaxial to the previous N45° contractional deformation event and documents an inversion of the stress. We interpret this inversion, as well as the development of the normal faults occurring at San Bartolomeo, as the onset of a tensional stress by bending moment. These structural features can be tentatively explained by the out-of-sequence reactivation of a deep basement structure, which would have deformed the area of the San Bartolomeo Hill in a broad antiform. Within this structure, the San Bartolomeo Hill Formation should lie in the summit because of its subhorizontal bedding attitude. The following N305° extensional event testifies to a further rotation of the stress field, which, however, continued to trigger the growth of the San Bartolomeo Hill structure. The N305°-directed bending moment is driven by a NW-directed horizontal σ1, in good agreement with the maximum stress calculated at Sant'Ambrogio and Sirmione at least since the Gelasian (see following).

In the eastern sector, the following events are reconstructed:

(1) Pre-Gelasian subsidence and deposition of the Montecio Conglomerate: The occurrence of Gelasian microfauna within the Montecio Conglomerate weathered gravels, provides a *terminus ante quem* for the deposition of the Montecio Conglomerate. The thickness of the deposit at Sant'Ambrogio (~50 m) suggests subsidence settings consistent with those occurring during the intra-Zanclean phase (Ghielmi et al., 2010) and also observed a few tens of kilometers westward at the San Bartolomeo Hill.

(2) Gelasian faulting of the Montecio Conglomerate: Weathered Montecio Conglomerate is found to fill tectonic fractures at Rivoli in association with Gelasian microfauna. This evidence can support a tectonic activity during the Gelasian that created tensile joints, such as those observed in the Montecio Conglomerate at Sant'Ambrogio, and could have likely produced local "pull-apart" basins bounded by WNW- to NW-striking right-lateral faults, such as the Cà Verde depression. This deformation was produced by a stress field with NNW horizontal σ1. The Sant'Ambrogio fault

shows some similarity in direction and deformation style with the Nogara fault detected in seismic lines. Their geometry and kinematics suggest that both belong to the same regional NW-directed "Schio-Vicenza"–like fault system.

In the central sector, the Sirmione Conglomerate recorded the youngest deformation event:

(1) Late Matuyama deposition of the Sirmione Conglomerate: The conglomerate was deposited during one of the earliest glacial stages occurring at the end of the early Pleistocene, likely in moderate- to low-subsidence settings.

(2) Middle Pleistocene faulting of the Sirmione Conglomerate: Due to the latest early Pleistocene age of the Sirmione Conglomerate, we refer the faulting of the Sirmione Conglomerate to the right following the middle Pleistocene. The NNE-directed fault observed at Villa Cortine in the Sirmione Conglomerate has roughly the same direction as the underlying Sirmione fault observed in the subsurface by means of seismic interpretation (Figs. 1 and 2A). Due to the poor exposures at Sirmione, it is still not possible to construct a complete picture of the structural relationship between both faults. Taking into account the widely documented left-lateral transpressive kinematics of the Giudicarie thrust belt (e.g., Picotti et al., 1995; Viganò et al., 2008), we propose as first interpretation that the left-lateral strike-slip fault observed at Villa Cortine may represent the surficial expression of the deeper Sirmione fault, for which we infer the same left-lateral transpressive kinematics observed in the Giudicarie belt.

On the whole, in our reconstruction of late Alpine tectonics in the Lake Garda area, we interpret three distinct deformation events (Fig. 10), recognized and distinguished by the different directions of compression and their timing of activity. The oldest corresponds to the intra-Zanclean event of Ghielmi et al. (2010), and it was produced by a severe northward migration of the Apennine fronts. The creation of accommodation space by flexure of the Alpine foreland during this event drove the deposition of the lower conglomerate (SB1) of the San Bartolomeo Hill Formation and, likely, the deposition of the Montecio Conglomerate a few tens of kilometers eastward. The marine transgression observed at San Bartolomeo with the SB2 clays marks the

maximum flooding surface relating to this event at ca. 4.0 Ma. The intra-Zanclean event can be interpreted according to Caputo et al. (2010) as a period of decoupling along the basal detachment layer of the Apennines critical taper, during which the convergence between the Apennines and Alps was accommodated by the frontal propagation of the Apennines thrusts, in agreement with what was observed in the subsurface (Ghielmi et al., 2010). The oldest event of contractional deformation observed in the SB1 conglomerate by Picotti et al. (1997) is parallel to the direction of the Northern Apennine migration, suggesting that, after the initial intra-Zanclean propagation of the Apennines thrusts, the stress was transferred through the Adria plate foreland and accommodated by the Alpine margin. This stress transfer is interpreted as resulting from coupling along the basal detachment of the Apennines critical taper. In this moment, we can constrain the onset of the uplift at the San Bartolomeo Hill and the oldest extensional deformation observed by Picotti et al. (1997). This event can be considered as a continuation of the intra-Zanclean deformation phase because the $\sigma 1$ value is roughly constant.

During the Gelasian, we observe a radical change of the $\sigma 1$ direction, which rotates from NE°(N50°) to NNW (~N172°–175°). Similar stress field variations have been documented in the eastern southern Alps during the last ~10 m.y. (Caputo et al., 2003). These variations are interpreted as temporary perturbations of the local stress field in the framework of the remote plate convergence between Africa and Europe and the northeastward migration of the Northern Apennines (Caputo et al., 2010). In this geodynamic settings, we interpret the Gelasian stress direction as a result of the vector sum between the stress induced by the NW-oriented Adria plate motion (Mazzoli and Helman, 1994) and the stress induced by the Apennine northeastward propagation. During the intra-Zanclean event, the latter was the most represented, whereas with the Gelasian event, we can assume that both stresses contributed almost equally to produce a NNW-oriented resultant vector for the observed $\sigma 1$. Probably due to the waning or a change in the deformation style of the Apennine tectonics, the Adria component gets more represented in the $\sigma 1$ final direction. This new stress regime led the Gelasian event to produce a further tilting in the

517 foreland (Apennine component of deformation) and in addition triggered the onset of strike-slip
518 kinematics in the Lake Garda area with the deformation of the Montecio Conglomerate along the
519 Sant'Ambrogio fault (Adria component of deformation). The youngest extensional deformation in
520 the San Bartolomeo Hill is roughly coaxial with this new NNW-directed σ1 and tentatively referred
521 to this event.

522 Data from the Sirmione Conglomerate show that the NNW-oriented σ1 was also acting
523 during the middle Pleistocene, when, in agreement with geomorphologic evidence (Desio, 1965;
524 Livio et al., 2009), tectonic deformation is documented in the Lake Garda area. The σ1 we calculate
525 for the Gelasian and middle Pleistocene events agrees with the direction of maximum compression
526 estimated from the mesostructural analyses in the eastern southern Alps (Caputo et al., 2010), thus
527 contributing to depict a regional scenario consistent over a distance of more than 200 km, from the
528 Tagliamento River (east) to the Lake Garda area (west).

529 **SEISMOTECTONIC IMPLICATIONS**

530 Our data from subsurface and land exposures led to the recognition of two sets of faults in
531 the Lake Garda area and the Mantova monocline. One set is characterized by NNE-trending thrust
532 faults, mostly represented in the western sector of the Lake Garda area and ascribable to the
533 Giudicarie belt. The second set is characterized by NW-trending strike-slip faults, observed in the
534 eastern sector and ascribable to a "Schio-Vicenza"–like system. In the Sirmione peninsula, macro-
535 and mesostructures belonging to both sets were observed. The NNE-directed and the NW-directed
536 fault sets bear left-transpressive and right-lateral strike-slip motion, respectively (Fig. 11, inset).
537 Our kinematic data are in agreement with the focal plane solutions and maximum horizontal
538 stresses provided by Viganò et al. (2008) and the Salò 2004 event (M_w = 5.0), which displayed a
539 left-transpressive motion (Fig. 11). In the seismotectonic perspective, earthquakes in the area of the
540 Lessini Mountains should be consistent with a right-lateral strike-slip reactivation of NW-directed
541 faults belonging to the Schio-Vicenza system.

North of Lake Garda, the structural style documented by Castellarin and Cantelli (2000) consists of a NW-directed set of the Schio-Vicenza faults deeply penetrating inside the Giudicarie belt (Fig. 1). The tens-of-kilometers-long, NW-directed transfer faults dissect the NNE-trending thrusts and anticlines in short segments, typically ~10 km or less (Fig. 1). We infer the same structural style in the Lake Garda area, where the NNE-directed Giudicarie thrusts may be likely segmented by the NW-trending "Schio-Vicenza"–like faults detected in the subsurface (i.e., the Nogara fault) as well as in land exposures (i.e., the Sant'Ambrogio fault). These NW faults can be interpreted as ancient (Mesozoic?) structures reactivated in the frame of the foreland deformation and kinematically associated with the NNE-directed thrusts of the Lake Garda area (Sirmione and Solferino faults). On the whole, the interplay between the two systems leads to the activation of relatively short NNE thrust ramps bounded by longer NW transfer faults with right-lateral strike-slip motion (Fig. 11, inset).

The western sector of Lake Garda has experienced earthquakes in the last centuries with comparable levels of damage and estimated M_w ranging from 4.6 to 5.5 (Pessina et al., 2013; Fig. 11). The empirical translation of these magnitudes in source length allows estimation of thrust ramps with lengths not exceeding 7 km (Wells and Coppersmith, 1994). The instrumental parameters of the last event in Salò 2004 (M_w = 5.0) point to thrust kinematics with a slight left-lateral component. Beside the Salò 2004 earthquake, a fragment of the same NNE-trending thrusts may have originated the 1901 earthquake (M_w = 5.5). In this context, even if the macroseismic epicenter of the A.D. 1222 earthquake (M_w = 5.8; Locati et al., 2011) was located in Lake Garda, recent paleoseismologic findings in the Monte Netto Hill (~10 km southeast of Brescia; Fig. 11) indicate the thrust systems in the Brescia area (Malpaga fault) as a probable causative source for this event (Livio et al., 2009).

In the seismic history of the Po Plain, the most destructive event occurred in A.D. 1117 (M_w = 6.7). Historical information about the damage distribution is sparse and defines significant effects in Cremona, Verona, and Padova, suggesting a very wide damage area (~150 km between Cremona

568 and Padova). A possible macroseismic epicenter has been proposed a few kilometers south of
569 Verona on the basis of historical data (Locati et al., 2011; Fig. 11). The definition of a seismogenic
570 source is still an open issue, as indicated by the occurrence of different hypotheses. According to
571 Galadini et al. (2005), the A.D. 1117 event can be associated to the Thiene-Bassano thrust, along
572 the front of the eastern southern Alps (Fig. 1). Galli (2005) supported a multi-epicentral hypothesis
573 involving the 1117 seismic sequence and the buried Piadena fault along the Apennine front (Fig.
574 11). Based on the empirical relationships of Wells and Coppersmith (1994), the estimated
575 magnitude of the A.D. 1117 earthquake was produced by a source of ~30–40 km of length,
576 compatible with the structural style of the Lessini Mountains block and the Mantova monocline,
577 where strike-slip faults are traceable for more than 30 km. For instance, the Nogara fault has been
578 traced on seismic lines for ~60 km, and the Sant'Ambrogio fault length is estimated at least ~30 km
579 (Fig. 11). As a result, therefore, we suggest that both faults should be regarded as a potential
580 candidate for the A.D. 1117 seismogenic source.

581 The Lessini Mountains block also represents the epicentral area of the A.D. 1891 earthquake
582 (M_w = 5.8). Although current hypotheses for the origin of this earthquake are not available, the
583 epicentral location in the innermost sector of Lessini Mountains suggests that it was originated by
584 the activation of one of the minor strike-slip faults related to the Schio-Vicenza system.

585 On the whole, by considering the structural framework discussed here and the distribution of
586 the seismicity, the interplay between NNE-directed Giudicarie thrusts and NW-directed "Schio-
587 Vicenza"–like faults is expected to generate moderate-magnitude earthquakes ($M_w < 6$) by the
588 activation of the former and stronger earthquakes (also $M_w > 6.5$) sourced on the latter.

589 **CONCLUSIONS**

590 The ongoing convergence between Africa and Europe, coupled with northward propagation
591 of Apennines thrusts, led to three different tectonic events during the last 5 m.y., namely the intra-
592 Zanclean, Gelasian, and middle Pleistocene. These events, formerly recognized in the subsurface of
593 the Po Plain, left a fingerprint also along the southern Alps margin. Pliocene deposits at San

Bartolomeo Hill and Sant'Ambrogio di Valpolicella recorded the oldest two deformations. The youngest event, formerly inferred by geomorphologic and paleoseismologic studies, has been observed and characterized in the Sirmione peninsula.

The intra-Zanclean event produced the southward flexure of the southern Alps and the marine transgression in the Alpine valleys at ca. 4.0 Ma. The associated stress was mainly Apennine-driven with a NE direction. Beginning in the Gelasian, the maximum compressive axis turned to the NNW, keeping this direction also during the middle Pleistocene. The associated deformation was accommodated by two sets of faults consisting of NNE-trending thrust faults, mostly represented in the western sector of the Lake Garda area and ascribable to the Giudicarie belt, and NW-trending strike-slip faults, observed in the eastern sector and ascribable to a "Schio-Vicenza"–like system. The interplay between these two sets of faults is interpreted to produce relatively short (<10 km length) thrust ramps activated in left transpression, bounded by relatively longer (30–60 km) transfer faults activated in a right-lateral strike-slip motion.

Based on our reconstruction, we expect moderate seismicity ($M_w < 6$) associated with the NNE-directed Giudicarie thrusts and stronger earthquakes (also $M_w > 6.5$) along the NW-trending "Schio-Vicenza"–like strike-slip faults. In this framework, the Nogara fault or the Sant'Ambrogio fault could be regarded as potential candidates for the A.D. 1117 earthquake seismogenic source.

ACKNOWLEDGMENTS

This research, developed and funded in the framework of the DPC-INGV **[[Please spell out DPC-INGV here.]]** 2007–2009 agreement (Project S1), benefited from useful discussions by C. Carcano, E. Castellaccio, D. Esu, E.M. Poli, B. Sala, D. Visonà, and R. Zorzin, to whom go our thanks. We also acknowledge ENI E&P for providing subsurface data and Giovanni Muttoni for welcoming Scardia to use the paleomagnetic facility at the Alpine Laboratory of Paleomagnetism. We are indebted to R. Cappelletto and M. Colombo for the access and kind permission for sampling in the Palace Hotel Villa Cortine estate. Paleostress was calculated with Faultkin (Marrett and Allmendinger, 1990; Allmendinger et al., 2012). Finally, we are

grateful to V. Picotti and Associate Editor Y. Dilek, whose thoughtful revisions greatly improved the manuscript.

REFERENCES CITED

[[Not cited?]]Allmendinger, R.W., Cardozo, N.C., and Fisher, D., 2012, Structural Geology Algorithms: Vectors & Tensors: Cambridge, UK, Cambridge University Press, 289 p.

Anderson, H., and Jackson, J.A., 1987, Active tectonics of the Adriatic region: Geophysical Journal of the Royal Astronomical Society, v. 91, p. 937–983, doi:10.1111/j.1365-246X.1987.tb01675.x.

Andrews, P., 1990, Owls, Caves and Fossils: Chicago, Illinois, University of Chicago Press, 231 p.

Backman, J., Raffi, I., Rio, D., Fornaciari, E., and Palike, H., 2012, Biozonation and biochronology of Miocene through Pleistocene calcareous nannofossils from low and middle latitudes: Newsletter on Stratigraphy, v. 45, p. 221–244, doi:10.1127/0078-0421/2012/0022.

Baroni, C., Bissolati, G., and Vercesi, P.L., 1995, Carta Geologica delle Prealpi Bresciane tra la Val Vrenda e il M. Pizzocolo: Atti Ticinesi Scienze della Terra, v. 38, 1 sheet. **[[Scale?]]**

Bellucci, L., Bona, F., Corrado, P., Magri, D., Mazzini, I., Parenti, F., Scardia, G., and Sardella, R., 2014, Evidence of late Gelasian dispersal of African fauna at Coste San Giacomo (Anagni Basin, central Italy): Quaternary Science Reviews (in press), doi:10.1016/j.quascirev.2013.10.011.

Bertini, A., 2001, Pliocene climatic cycles and altitudinal forest development from 2.7 Ma in the Northern Apennines (Italy): Evidence from the pollen record of the Stirone section (c. 5.1 to c. 2.2 Ma): Geobios, v. 34, p. 253–265, doi:10.1016/S0016-6995(01)80074-7.

Bertotti, G., Picotti, V., Bernoulli, D., and Castellarin, A., 1993, From rifting to drifting: Tectonic evolution of the South-Alpine upper crust from the Triassic to the Early Cretaceous: Sedimentary Geology, v. 86, p. 53–76, doi:10.1016/0037-0738(93)90133-P.

644 Brambilla, G., and Lualdi, A., 1986, Il Pliocene della Provincia di Bergamo (Italia settentrionale).
645 Analisi faunistica ed inquadramento cronologico e paleoambientale: Bollettino della Società
646 Paleontologica Italiana, v. 25, p. 237–266.
647 Burrato, P., Vannoli, P., Fracassi, U., and Basili, R., 2012, Is blind faulting truly invisible?
648 Tectonic-controlled drainage evolution in the epicentral area of the May 2012, Emilia-
649 Romagna earthquake sequence (northern Italy): Annals of Geophysics, v. 55, p. 525–531.
650 Caputo, R., Poli, M.E., and Zanferrari, A., 2003, Neogene-Quaternary twist tectonics in the eastern
651 southern Alps, Italy: Memorie di Scienze Geologiche, v. 54, p. 155–158.
652 Caputo, R., Poli, M.E., and Zanferrari, A., 2010, Neogene-Quaternary tectonic stratigraphy of the
653 eastern southern Alps, NE Italy: Journal of Structural Geology, v. 32, p. 1009–1027,
654 doi:10.1016/j.jsg.2010.06.004.
655 Carton, A., and Castaldini, D., 1985, Approfondimenti di morfotettonica tra il Lago di Garda ed il
656 Torrente Alpone (Provincia di Verona): Bollettino del Museo Civico di Storia Naturale di
657 Verona, v. 12, p. 461–491.
658 Cassinis, G., and Perotti, C.R., 1996, Connection between late Variscan lineaments and Alpine
659 tectonic evolution in central southern Alps (Italy): A short review: Notes et Mémoires du
660 Service Géologique Maroc, v. 387, p. 125–134.
661 Castellaccio, E., and Zorzin, R., eds., 2012, Acque Calde e Geotermia della Provincia di Verona:
662 Memorie del Museo Civico di Storia Naturale di Verona 8, 176 p.
663 Castellarin, A., and Cantelli, L., 2000, Neo-Alpine evolution of the southern eastern Alps: Journal
664 of Geodynamics, v. 30, p. 251–274, doi:10.1016/S0264-3707(99)00036-8.
665 Castellarin, A., Cantelli, L., Fesce, A.M., Mercier, J.L., Picotti, V., Pini, G.A., Prosser, G., and
666 Selli, L., 1992, Alpine compressional tectonics in the southern Alps: Relationships with the N-
667 Apennines: Annales Tectonicae, v. 6, p. 62–94.
668 Cita, M.B., 1949, L'affioramento neocretaceo di Sirmione e la sua microfauna: Rivista Italiana di
669 Paleontologia e Stratigrafia, v. 55, p. 121–134.

Cita, M.B., 1955, Paleogeografia del Terziario nella regione Gardesana: Rivista Italiana di Paleontologia e Stratigrafia, v. 61, p. 137–161.

Corselli, C., Cremaschi, M., and Violanti, D., 1985, Il canyon messiniano di Malnate (Varese), pedogenesi tardo miocenica ed ingressione marina pliocenica al margine meridionale delle Alpi: Rivista Italiana di Paleontologia e Stratigrafia, v. 91, p. 215–236.

Cremaschi, M., 1987, Paleosols and Vetusols in the Central Po Plain (Northern Italy): Milano, Edizioni Unicopli, 306 p.

D'Agostino, N., Avallone, A., Cheloni, D., D'Anastasio, E., Mantenuto, S., and Selvaggi, G., 2008, Active tectonics of the Adriatic region from GPS and earthquake slip vectors: Journal of Geophysical Research, v. 113, p. B12413, doi:10.1029/2008JB005860.

Desio, A., 1965, I rilievi isolati della pianura lombarda ed i movimenti tettonici del Quaternario: Rendiconti dell'Istituto Lombardo Accademia di Scienze e Lettere A, v. 99, p. 881–894.

Esu, D., 1980, Neogene freshwater gastropods and their evolution in the Western Mediterranean area: Geologica Romana, v. 19, p. 231–249.

Fantoni, R., and Franciosi, R., 2010, Tectono-sedimentary setting of the Po Plain and Adriatic foreland: Rendiconti Lincei, v. 21, p. 197–209, doi:10.1007/s12210-010-0102-4.

Fantoni, R., Bersezio, R., and Forcella, F., 2004, Alpine structure and deformation chronology at the southern Alps–Po Plain border in Lombardy: Bollettino della Società Geologica Italiana, v. 123, p. 463–476.

Favero, V., and Grandesso, P., 1982, Nuovi affioramenti di Pliocene marino nei dintorni di Bassano del Grappa (Vicenza): Memorie della Societa Geologica Italiana, v. 24, p. 71–77.

Galadini, F., and Galli, P., 1999, Palaeoseismology related to the displaced Roman archaeological remains at Egna (Adige Valley, northern Italy): Tectonophysics, v. 308, p. 171–191, doi:10.1016/S0040-1951(99)00080-3.

694 Galadini, F., Galli, P., Cittadini, A., and Giaccio, B., 2001, Late Quaternary fault movements in the
695 Mt. Baldo–Lessini Mts. sector of the south alpine area (northern Italy): Geologie en Mijnbouw
696 (Netherlands Journal of Geosciences), v. 80, p. 187–208.
697 Galadini, F., Poli, M.E., and Zanferrari, A., 2005, Seismogenic sources potentially responsible for
698 earthquakes with M≥ 6 in the eastern southern Alps (Thiene-Udine sector, NE Italy):
699 Geophysical Journal International, v. 161, p. 739–762, doi:10.1111/j.1365-246X.2005.02571.x.
700 Galadini, F., Falcucci, E., Galli, P., Giaccio, B., Gori, S., Messina, P., Moro, M., Saroli, M.,
701 Scardia, G., and Sposato, A., 2012, Time intervals to assess active and capable faults for
702 engineering practices in Italy: Engineering Geology, v. 139–140, p. 50–65,
703 doi:10.1016/j.enggeo.2012.03.012.
704 Galli, P., 2005, I terremoti del Gennaio 1117. Ipotesi di un epicentro nel cremonese: Il Quaternario,
705 v. 18, p. 87–100.
706 Garzanti, E., Andò, S., and Vezzoli, G., 2006, The continental crust as a source of sand (southern
707 Alps cross section, northern Italy): The Journal of Geology, v. 114, p. 533–554,
708 doi:10.1086/506159.
709 Garzanti, E., Vezzoli, G., and Andò, S., 2011, Paleogeographic and paleodrainage changes during
710 Pleistocene glaciations (Po Plain, northern Italy): Earth-Science Reviews, v. 105, p. 25–48,
711 doi:10.1016/j.earscirev.2010.11.004.
712 Gazzi, P., Zuffa, G.G., Gandolfi, G., and Paganelli, L., 1973, Provenienza e dispersione litoranea
713 delle sabbie delle spiagge adriatiche fra le foci dell'Isonzo e del Foglia: Inquadramento
714 regionale: Memorie della Societa Geologica Italiana, v. 12, p. 1–37.
715 Ghielmi, M., Minervini, M., Nini, C., Rogledi, S., Rossi, M., and Vignolo, A., 2010, Sedimentary
716 and tectonic evolution in the eastern Po Plain and northern Adriatic Sea area from Messinian to
717 middle Pleistocene (Italy): Rendiconti Lincei, v. 21, p. 131–166, doi:10.1007/s12210-010-
718 0101-5.

719 Gibbard, P.L., Head, M.J., and Walker, M.J.C., 2010, Formal ratification of the Quaternary
720 System/Period and the Pleistocene Series/Epoch with a base at 2.58 Ma: Journal of Quaternary
721 Science, v. 25, p. 96–102, doi:10.1002/jqs.1338.
722 Laubscher, H., 1985, Large-scale, thin-skinned thrusting in the southern Alps: Kinematic models:
723 Geological Society of America Bulletin, v. 96, p. 710–718, doi:10.1130/0016-
724 7606(1985)96<710:LTTITS>2.0.CO;2.
725 Livio, F., Berlusconi, A., Michetti, A.M., Sileo, G., Zerboni, A., Trombino, L., Cremaschi, M.,
726 Mueller, K., Vittori, E., Carcano, C., and Rogledi, S., 2009, Active fault-related folding in the
727 epicentral area of the December 25, 1222 (I_o = IX MCS), Brescia earthquake (northern Italy):
728 Seismotectonic implications: Tectonophysics, v. 476, p. 320–335,
729 doi:10.1016/j.tecto.2009.03.019.
730 Locati, M., Camassi, R., and Stucchi, M., eds., 2011, DBMI11, the 2011 version of the Italian
731 Macroseismic Database: http://emidius.mi.ingv.it/DBMI11 (accessed May 2014),
732 doi:10.6092/INGV.IT-DBMI11.
733 Lourens, L.J., Hilgen, F.J., Laskar, J., Shackleton, N.J., and Wilson, D.S., 2005, The Neogene
734 Period, *in* Gradstein, F.M., Ogg, J.G., and Smith, A.G., eds., A Geologic Time Scale 2004:
735 Cambridge, UK, Cambridge University Press, p. 409–440.
736 **[[Not cited?]]**Marrett, R.A., and Allmendinger, R.W., 1990, Kinematic analysis of fault-slip data:
737 Journal of Structural Geology, v. 12, p. 973–986, doi:10.1016/0191-8141(90)90093-E.
738 Martini, E., 1971, Standard Tertiary and Quaternary calcareous nannoplankton zonation, *in*
739 Farinacci, A., ed., Proceedings of the 2nd International Conference Planktonic Microfossils
740 Roma: Rome, Ed. Tecnosci, v. 2, p. 739–785.
741 Mazzoli, S., and Helman, M., 1994, Neogene patterns of relative plate motion for Africa-Europe:
742 Some implications for recent central Mediterranean tectonics: Geologische Rundschau, v. 83,
743 p. 464–468.

McFadden, P.L., and McElhinny, M.W., 1988, The combined analysis of remagnetization circles and direct observations in paleomagnetism: Earth and Planetary Science Letters, v. 87, p. 161–172, doi:10.1016/0012-821X(88)90072-6.

[[City of publication?]]Miall, A.D., 2006, The Geology of Fluvial Deposits: Springer, 582 p.

Monegato, G., Stefani, C., and Zattin, M., 2010, From present rivers to old terrigenous sediments: The evolution of the drainage system in the eastern southern Alps: Terra Nova, v. 22, p. 218–226, doi:10.1111/j.1365-3121.2010.00937.x.

Muttoni, G., Carcano, C., Garzanti, E., Ghielmi, M., Piccin, A., Pini, R., Rogledi, S., and Sciunnach, D., 2003, Onset of major Pleistocene glaciations in the Alps: Geology, v. 31, p. 989–992, doi:10.1130/G19445.1.

Muttoni, G., Ravazzi, C., Breda, M., Pini, R., Laj, C., Kissel, C., Mazaud, A., and Garzanti, E., 2007, Magnetostratigraphic dating of an intensification of glacial activity in the southern Italian Alps during marine isotope stage 22: Quaternary Research, v. 67, p. 161–173, doi:10.1016/j.yqres.2006.07.006.

Nomade, S., Pastre, J.-F., Guillou, H., Faure, M., Guérin, C., Delson, E., Debard, E., Voinchet, P., and Messager, E., 2014, $^{40}Ar/^{39}Ar$ constraints on some French landmark late Pliocene to early Pleistocene large mammalian paleofaunas: Paleoenvironmental and paleoecological implications: Quaternary Geochronology, v. 21, p. 2–15, doi:10.1016/j.quageo.2012.12.006.

Pessina, V., Tertulliani, A., Camassi, R., Rossi, A., and Scardia, G., 2013, The revision of the October 30, 1901, earthquake, west of Lake Garda (northern Italy): Bollettino di Geofisica Teorica ed Applicata, v. 54, p. 77–110.

Picotti, V., and Pazzaglia, F.J., 2008, A new active tectonic model for the construction of the Northern Apennines mountain front near Bologna (Italy): Journal of Geophysical Research, v. 113, p. B08412, doi:10.1029/2007JB005307.

Picotti, V., Prosser, G., and Castellarin, A., 1995, Structures and kinematics of the Giudicarie–Val Trompia fold and thrust belt (central southern Alps, northern Italy): Memorie di Scienze Geologiche, v. 47, p. 95–109.

Picotti, V., Bertotti, G., Capozzi, R., and Fesce, A.M., 1997, Evoluzione tettonica quaternaria della Pianura Padana centro-orientale e dei suoi margini: Il Quaternario, v. 10, p. 513–520.

[[City of publication? Series title/type?]]Picotti, V., Capozzi, R., Bertozzi, G., Mosca, F., Sitta, A., and Tornaghi, M., 2007, The Miocene petroleum system of the Northern Apennines in the central Po Plain (Italy), *in* Lacombe, O., Roure, F., Lavé, J., and Vergés, J., eds., Thrust Belts and Foreland Basins: Springer, v. 15, p. 117–131, doi:10.1007/978-3-540-69426-7_6.

Pieri, M., and Groppi, G., 1981, Subsurface Geological Structure of the Po Plain, Italy: Consiglio Nazionale delle Ricerche, Progetto Finalizzato Geodinamica 414, 13 p.

Raffi, I., and Rio, D., 1978, Il nannoplancton calcareo dell'affioramento pliocenico di Cornuda (Veneto): Acta Naturalia de l'Ateneo Parmense, v. 14, p. 81–94.

Ravaglia, A., Seno, S., Toscani, G., and Fantoni, R., 2006, Mesozoic extension controlling the southern Alps thrust front geometry under the Po Plain, Italy: Insights from sandbox models: Journal of Structural Geology, v. 28, p. 2084–2096, doi:10.1016/j.jsg.2006.07.011.

Ravazzi, C., and Rossignol Strick, M., 1995, Vegetation change in a climatic cycle of early Pleistocene age in the Leffe Basin (northern Italy): Palaeogeography, Palaeoclimatology, Palaeoecology, v. 117, p. 105–122, doi:10.1016/0031-0182(94)00118-R.

Sala, B., Masini, F., and Torre, D., 1994, Villanyian arvicolids from Rivoli Veronese, a karst fissure in the Adige Valley, northeastern Italy: Bollettino della Società Paleontologica Italiana, v. 33, p. 3–11.

Scardia, G., Muttoni, G., and Sciunnach, D., 2006, Subsurface magnetostratigraphy of Pleistocene sediments from the Po Plain (Italy): Constraints on rates of sedimentation and rock uplift: Geological Society of America Bulletin, v. 118, p. 1299–1312, doi:10.1130/B25869.1.

Scardia, G., Donegana, M., Muttoni, G., Ravazzi, C., and Vezzoli, G., 2010, Late Matuyama climate forcing on sedimentation at the margin of the southern Alps (Italy): Quaternary Science Reviews, v. 29, p. 832–846, doi:10.1016/j.quascirev.2009.12.002.

Scardia, G., De Franco, R., Muttoni, G., Rogledi, S., Caielli, G., Carcano, C., Sciunnach, D., and Piccin, A., 2012, Stratigraphic evidence of a middle Pleistocene climate-driven flexural uplift in the Alps: Tectonics, v. 31, TC6004, doi:10.1029/2012TC003108.

Sissingh, W., 1977, Biostratigraphy of Cretaceous calcareous nannoplankton: Geologie en Mijnbouw, v. 56, p. 37–65.

Venzo, S., 1957, Rilevamento Geologico dell'Anfiteatro Morenico del Garda: Parte I: Memorie della Società Italiana di Scienze Naturali e del Museo Civico di Storia Naturale di Milano, v. 12, 140 p.

Venzo, S., 1961, Rilevamento Geologico dell'Anfiteatro Morenico del Garda: Parte II: Memorie della Società Italiana di Scienze Naturali e del Museo Civico di Storia Naturale di Milano, v. 13, 64 p.

Venzo, S., 1965, Rilevamento Geologico dell'Anfiteatro Morenico Frontale del Garda dal Chiese all'Adige: Memorie della Società Italiana di Scienze Naturali e del Museo Civico di Storia Naturale di Milano, v. 14, 82 p.

Viganò, A., Bressan, G., Ranalli, G., and Martin, S., 2008, Focal mechanism inversion in the Giudicarie-Lessini seismotectonic region (southern Alps, Italy): Insights on tectonic stress and strain: Tectonophysics, v. 460, p. 106–115, doi:10.1016/j.tecto.2008.07.008.

Wells, D.L., and Coppersmith, K.J., 1994, New empirical relationships among magnitude, rupture length, rupture width, rupture area, and surface displacement: Bulletin of the Seismological Society of America, v. 84, p. 974–1002.

SCIENCE EDITOR: NANCY RIGGS

ASSOCIATE EDITOR: YILDIRIM DILEK

MANUSCRIPT RECEIVED 4 SEPTEMBER 2013

REVISED MANUSCRIPT RECEIVED 12 MAY 2014

MANUSCRIPT ACCEPTED ___ MONTH 2014

Printed in the USA

FIGURE CAPTIONS

Figure 1. Structural map of the central-eastern Po Plain with the track of seismic lines A and B, and the Rodigo 1 well (black square) shown in Figure 2. Stars indicate the land exposures where stratigraphic and structural observations were carried out (SB—San Bartolomeo Hill; SIR—Sirmione peninsula; SA—Sant'Ambrogio di Valpolicella).

Figure 2. Representative seismic profiles from the Po Plain and related stratigraphic interpretation. The Rodigo 1 and water wells (*w*) used to calibrate the uppermost seismic horizons are also displayed. Ages of biostratigraphic events are from Lourens et al. (2005). **[[Figure edit: Define genus abbreviations in caption.]]**

Figure 3. Geologic sketch, stratigraphy, and biostratigraphic data of the San Bartolomeo Hill Formation. Pollen percentages are based on a sum including pollen in primary deposition of trees, shrubs, and upland herbs. **[[Figure edits: Add lat and long to A. Add legend for patterns in lithostratigraphy column? Define P. genus abbreviation in caption.]]**

Figure 4. Ternary diagram showing the petrographic composition of sediments coming from the study sites, compared to Pleistocene fluvioglacial sample and the main source areas represented in 90% confidence field (data from Gazzi et al., 1973; Garzanti et al., 2006, 2011; Monegato et al., 2010).

Figure 5. (A) Geologic sketch of the eastern sector of the Lake Garda area. (B) Geologic map of the Sant'Ambrogio area. Hatches on the faults indicate the dip of the plane; stars indicate the sites where structural observations were carried out. (C) Mesoscale data (Schmidt net, lower hemisphere)

of main faults, joints, and deformed pebbles. Black arrows represent the σ1 direction calculated from the structural measurements. **[[Figure edit: Add lat and long to A and B.]]**

Figure 6. Evidence of tectonic deformation in the Montecio Conglomerate: (A–B) Parallel striae on a flat and polished surface of a pebble (A; pen for scale) related to the WNW fault system, indicated by black arrows in B (Montecio locality, NE of Sant'Ambrogio). (C) High-angle, N-dipping, normal fault consisting of two main surfaces (white arrows) that bound a 50-cm-thick fault breccia (Montecio locality); S-C shears are indicated by black lines. (D) E-NE–striking open fracture filled by the weathered Montecio Conglomerate at Rivoli V.se. **[[Spell out V.se. here.]]**

Figure 7. Geologic map of the Sirmione peninsula. Stars indicate the sites where structural observations were carried out. Insets at the top: Mesoscale data (Schmidt net, lower hemisphere) of main faults and deformed pebbles. Black arrows represent the σ1 direction calculated from the structural measurements. **[[Figure edits: Add lat and long. Fix spelling of Cretaceous in cherty limestone legend text.]]**

Figure 8. Stratigraphy, paleomagnetism, and pollen data from the Sirmione Conglomerate. The pelitic level where samples for paleomagnetism and pollen analysis were collected is indicated by arrow. Paleomagnetism: open and closed symbols in the orthogonal vector diagram represent projections onto vertical and horizontal plane, respectively; open and closed symbols in the equal-area projection represent projections onto upper and lower hemisphere, respectively. Star is the site mean value. Pollen percentages are based on a sum including pollen in primary deposition of trees, shrubs, and upland herbs. Xerophytes = sum of *Artemisia*, *Ephedra fragilis*, and *Ephedra distachya* types, *Hippophae*, *Centaurea scabiosa*, *Helianthemum*, Chenopodiaceae; upland herbs = sum of all terrestrial angiosperms, herbaceous xerophytes excluded. ChRM—characteristic remanent magnetization. **[[Figure edits: Fix spelling of palynomorphs (right bottom graph). Add legend for patterns used in lithostratigraphy column?]]**

Figure 9. Evidence of tectonic deformation in the Sirmione peninsula: (A) Left-lateral, NE-striking, high-angle fault zone at Villa Cortine, consisting of several-meters-long anastomosed faults (black

lines) and depicting small-scale flower structures (hammer as scale). Secondary extensional component of movement is shown by the displacement of bedding surfaces (dashed white lines). (B) NE-striking and left-lateral fault, consisting of a decimeters-wide shear zone internally characterized by anastomosed fault surfaces (Villa Cortine locality). (C) Aerial photograph of the northern end of the Sirmione peninsula, showing NW-striking, strike-slip fault system and the NNE-striking bedding attitude. Note the northeastern horsetail termination of the NW fault system. (D) Line drawing of panel C.

Figure 10. Synthetic diagram showing deformation and age of the tectonic events recognized in the subsurface of the Po Plain (Ghielmi et al., 2010) and along the southern Alps margin in the Lake Garda area (this study). The direction of maximum compression estimated from the mesostructural analyses ($\sigma 1$) is also reported. **[[Figure edits: Define genus abbreviations and ATNTS in caption.]]**

Figure 11. Seismotectonic model of the central Po Plain. Faults displaying activity during the Pleistocene are reported from Galadini et al. (2001), Galli (2005), Livio et al. (2009), and this study. The focal plane solutions are from Viganò et al. (2008); macroseismic epicenters of historical earthquakes (squares) are from DBMI11 (Locati et al., 2011). The pressure-temperature (P-T) diagrams for Sirmione and Sant'Ambrogio (in gray) were calculated from the structural and kinematics data presented in Figures 5 and 7. Crosses indicate the isolated reliefs of the Po Plain produced by active fault-related folding. Shaded area shows the vent of hot waters after Castellaccio and Zorzin (2012). Inset at the lower-left corner: structural sketch of the interplay between the NNE-trending Giudicarie thrusts and the NW-trending strike-slip faults produced by the middle Pleistocene maximum compression axis ($\sigma 1$). **[[Figure edits: Add lat and long to map.]]**

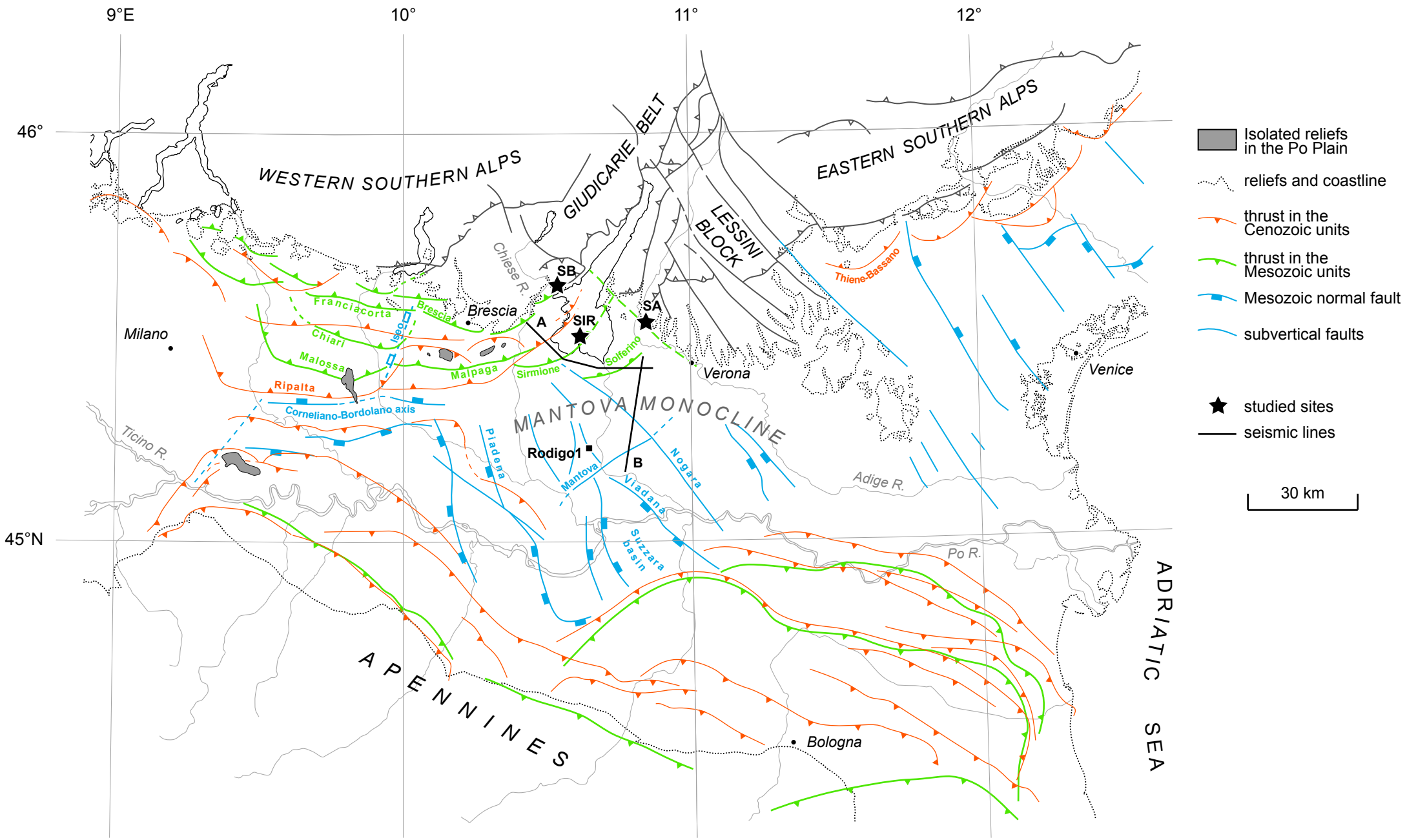
9°E
10°
11°
12°
46°
45°N
WESTERN SOUTHERN ALPS
GIUDICARIE BELT
LESSINI BLOCK
EASTERN SOUTHERN ALPS
APENNINES
ADRIATIC SEA
MANTOVA MONOCLINE
Milano
Brescia
Verona
Venice
Bologna
Ticino R.
Chiese R.
Adige R.
Po R.
SB
SIR
SA
A
B
Rodigo1
Franciacorta
Brescia
Chiari
Iseo
Malossa
Malpaga
Sirmione
Solferino
Ripalta
Corneliano-Bordolano axis
Piadena
Mantova
Viadana
Nogara
Suzzara basin
Thiene-Bassano
Isolated reliefs in the Po Plain
reliefs and coastline
thrust in the Cenozoic units
thrust in the Mesozoic units
Mesozoic normal fault
subvertical faults
studied sites
seismic lines
30 km

Figure 1

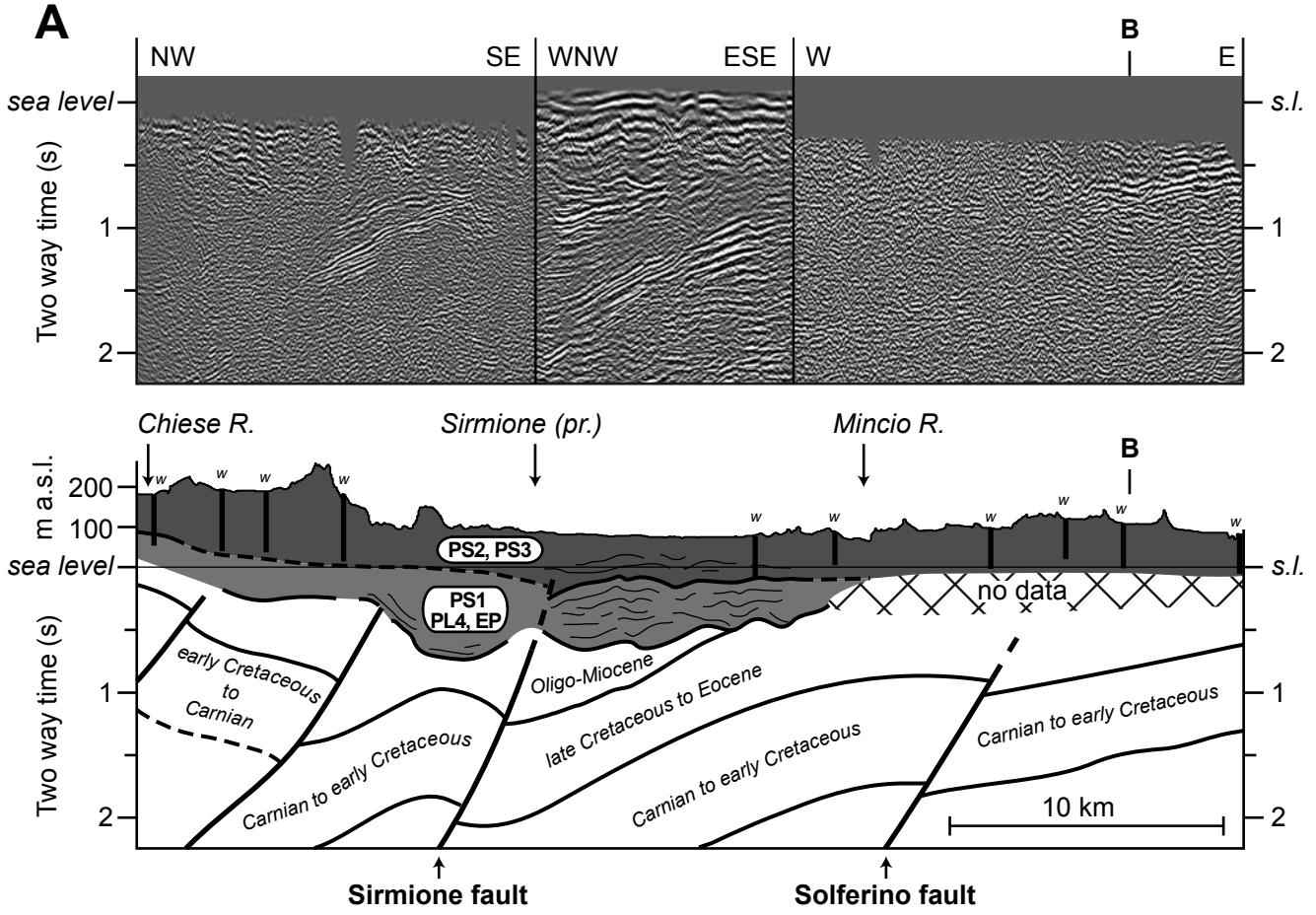
A
NW
SE
WNW
ESE
W
B
E
sea level
s.l.
Two way time (s)
1
2
Chiese R.
Sirmione (pr.)
Mincio R.
m a.s.l.
200
100
PS2, PS3
PS1
PL4, EP
no data
early Cretaceous to Carnian
Carnian to early Cretaceous
Oligo-Miocene
late Cretaceous to Eocene
Carnian to early Cretaceous
Carnian to early Cretaceous
10 km
Sirmione fault
Solferino fault

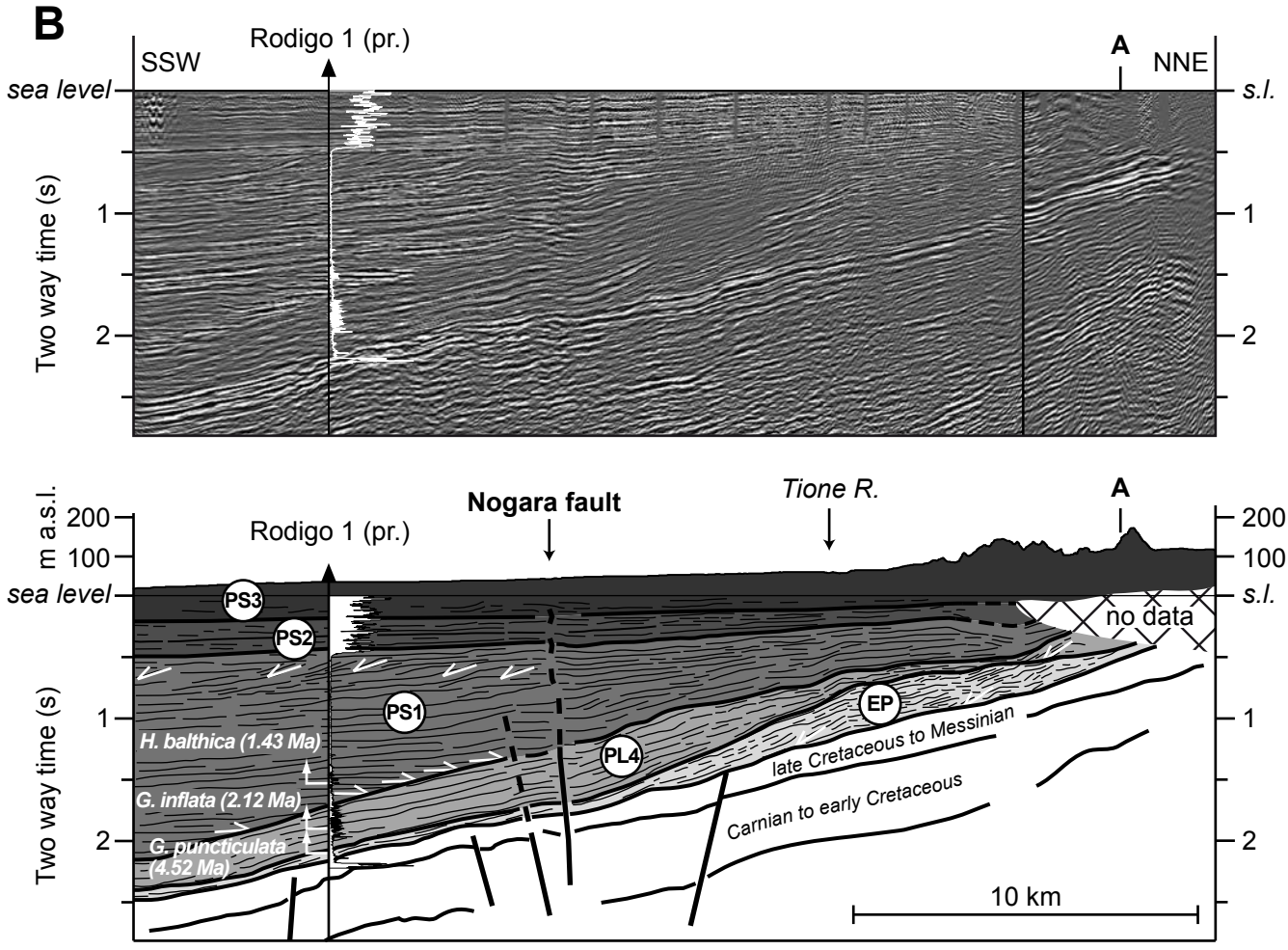
B
SSW
Rodigo 1 (pr.)
A
NNE
sea level
s.l.
Two way time (s)
1
2
m a.s.l.
200
100
Nogara fault
Tione R.
PS3
PS2
PS1
EP
PL4
no data
H. balthica (1.43 Ma)
G. inflata (2.12 Ma)
G. puncticulata (4.52 Ma)
late Cretaceous to Messinian
Carnian to early Cretaceous
10 km

Figure 2

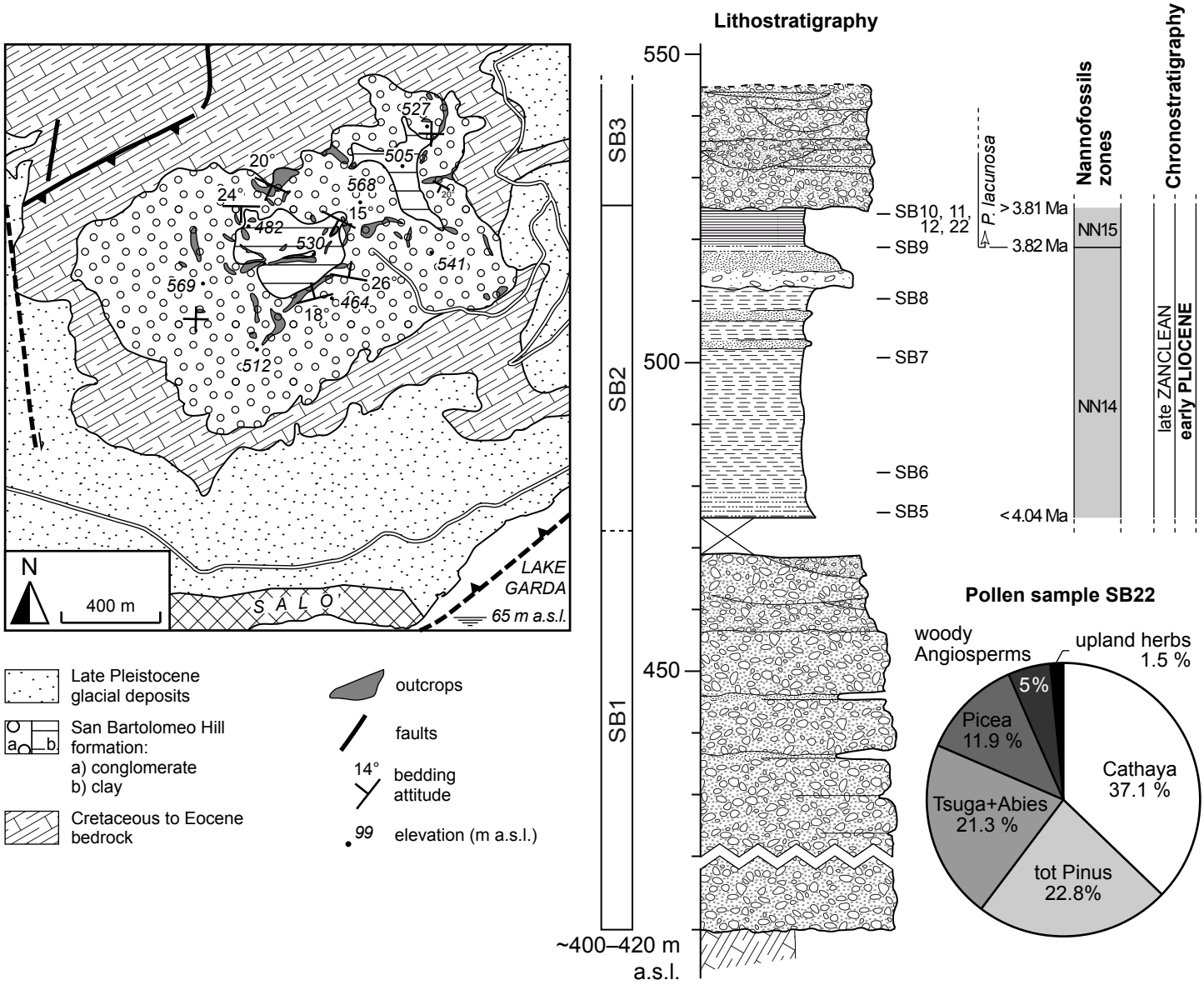
Lithostratigraphy
550
500
450
~400–420 m a.s.l.
SB3
SB2
SB1
SB10, 11, 12, 22
SB9
SB8
SB7
SB6
SB5
P. lacunosa
> 3.81 Ma
3.82 Ma
< 4.04 Ma
Nannofossils zones
NN15
NN14
Chronostratigraphy
late ZANCLEAN
early PLIOCENE
N
400 m
LAKE GARDA
65 m a.s.l.
S A L Ò
527
505
568
482
530
541
569
464
512
20°
24°
15°
26°
18°
Late Pleistocene glacial deposits
San Bartolomeo Hill formation:
a) conglomerate
b) clay
Cretaceous to Eocene bedrock
outcrops
faults
14° bedding attitude
99 elevation (m a.s.l.)
Pollen sample SB22
woody Angiosperms
upland herbs 1.5 %
5%
Picea 11.9 %
Cathaya 37.1 %
Tsuga+Abies 21.3 %
tot Pinus 22.8%

Figure 3

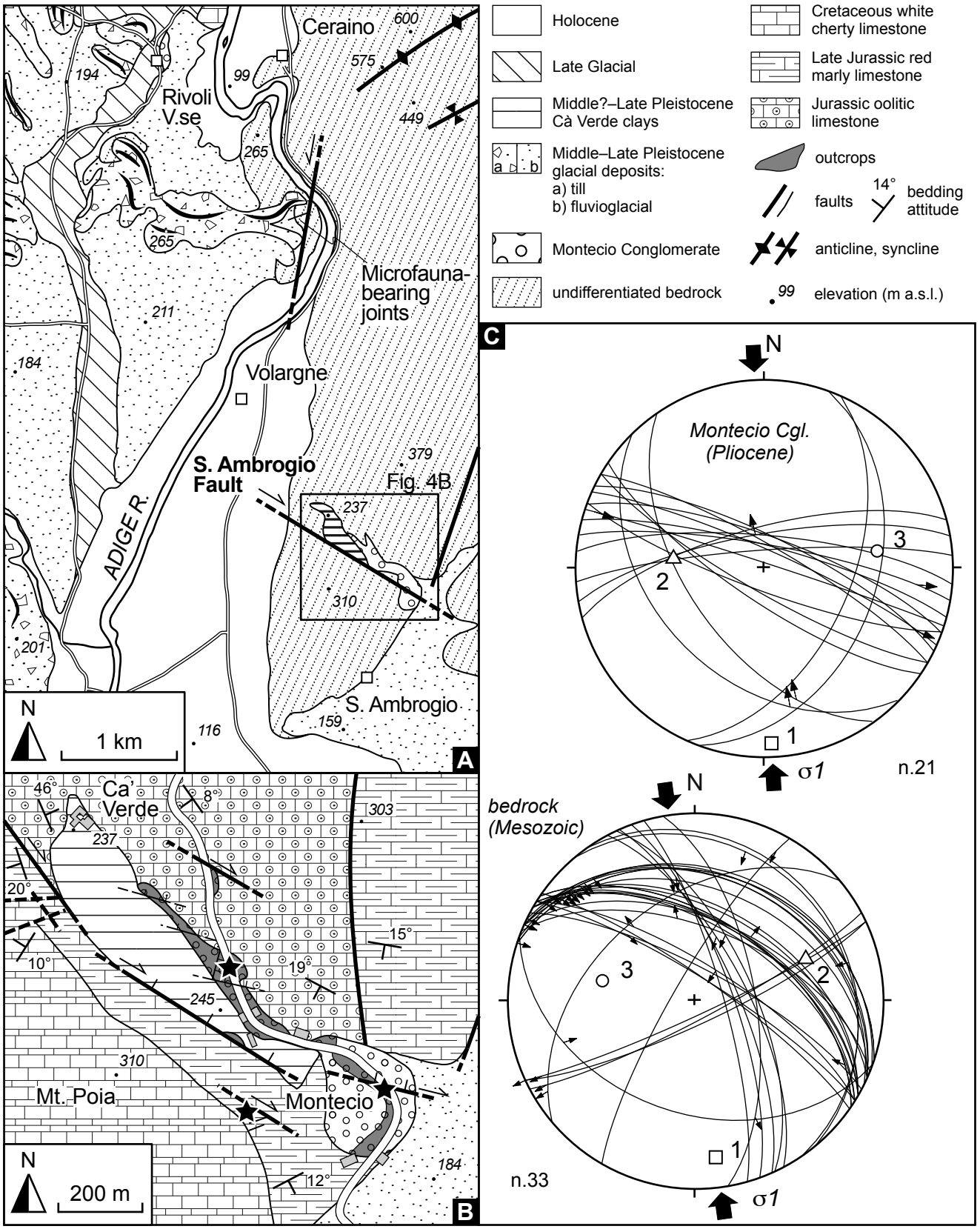
Ceraino
600
575
449
194
99
Rivoli
V.se
265
265
211
184
Microfauna-
bearing
joints
Volargne
379
S. Ambrogio
Fault
Fig. 4B
237
310
ADIGE R.
201
116
159
S. Ambrogio
N
1 km
A
46°
Ca'
Verde
8°
303
237
20°
15°
10°
19°
245
310
Mt. Poia
Montecio
12°
184
N
200 m
B
Holocene
Late Glacial
Middle?–Late Pleistocene
Cà Verde clays
Middle–Late Pleistocene
glacial deposits:
a) till
b) fluvioglacial
Montecio Conglomerate
undifferentiated bedrock
Cretaceous white
cherty limestone
Late Jurassic red
marly limestone
Jurassic oolitic
limestone
outcrops
faults
14°
bedding
attitude
anticline, syncline
99
elevation (m a.s.l.)
C
N
Montecio Cgl.
(Pliocene)
3
2
1
σ1
n.21
N
bedrock
(Mesozoic)
3
2
1
σ1
n.33

Figure 4

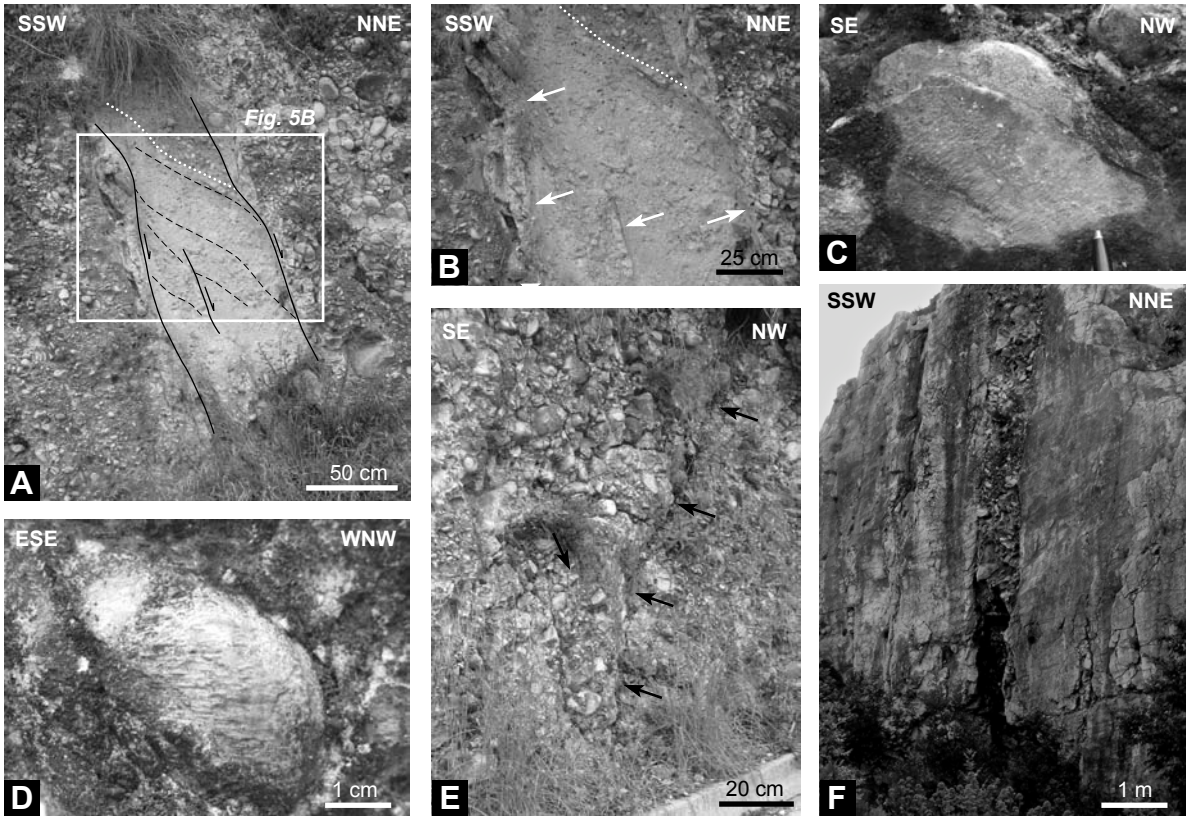
SSW
NNE
Fig. 5B
50 cm
A
SSW
NNE
25 cm
B
SE
NW
C
ESE
WNW
1 cm
D
SE
NW
20 cm
E
SSW
NNE
1 m
F

Figure 5

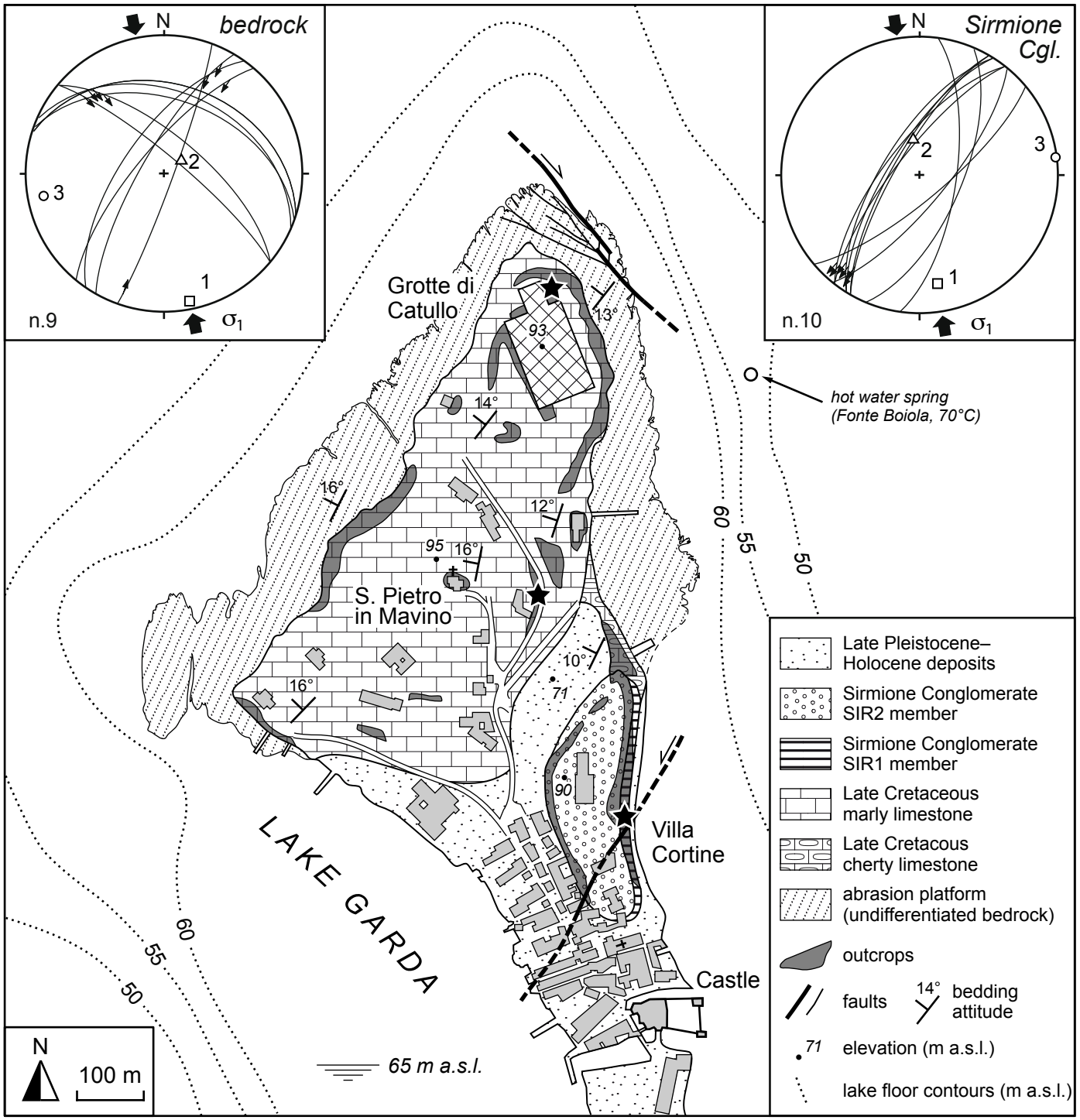
N
bedrock
3
2
1
n.9
σ1
N
Sirmione
Cgl.
2
3
1
n.10
σ1
Grotte di
Catullo
93
13°
14°
16°
12°
95
16°
S. Pietro
in Mavino
10°
71
16°
90
Villa
Cortine
Castle
LAKE GARDA
60
55
50
hot water spring
(Fonte Boiola, 70°C)
60
55
50
65 m a.s.l.
N
100 m
Late Pleistocene–
Holocene deposits
Sirmione Conglomerate
SIR2 member
Sirmione Conglomerate
SIR1 member
Late Cretaceous
marly limestone
Late Cretacous
cherty limestone
abrasion platform
(undifferentiated bedrock)
outcrops
faults
14°
bedding
attitude
71
elevation (m a.s.l.)
lake floor contours (m a.s.l.)

Figure 6

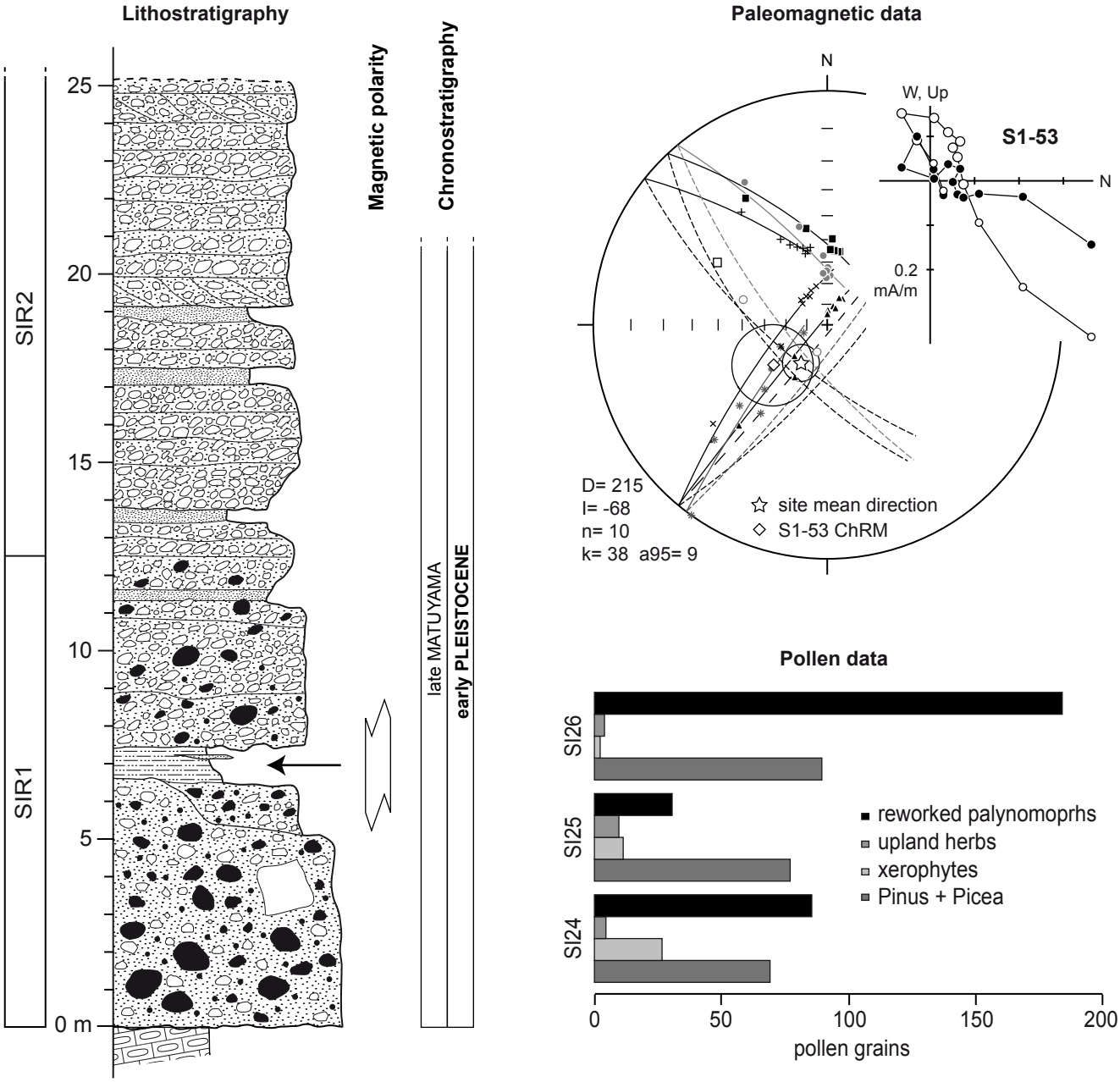
Lithostratigraphy
Magnetic polarity
Chronostratigraphy
SIR2
SIR1
25
20
15
10
5
0 m
late MATUYAMA
early PLEISTOCENE
Paleomagnetic data
N
W, Up
S1-53
N
0.2
mA/m
D= 215
I= -68
n= 10
k= 38 a95= 9
site mean direction
S1-53 ChRM
Pollen data
SI26
SI25
SI24
reworked palynomoprhs
upland herbs
xerophytes
Pinus + Picea
0
50
100
150
200
pollen grains

Figure 7

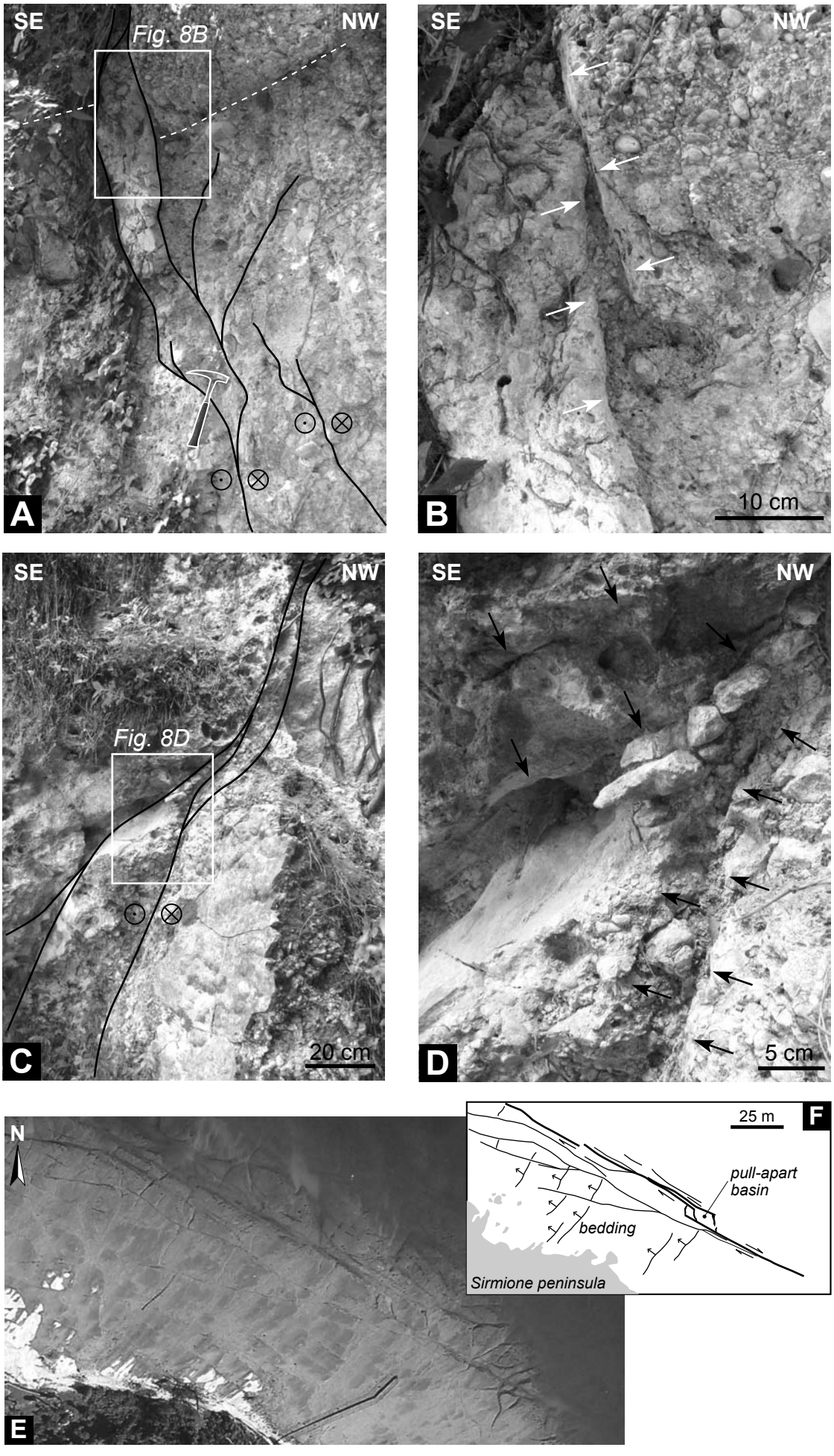
SE
NW
Fig. 8B
A
SE
NW
10 cm
B
SE
NW
Fig. 8D
20 cm
C
SE
NW
5 cm
D
N
E
25 m
F
pull-apart
basin
bedding
Sirmione peninsula

Figure 8

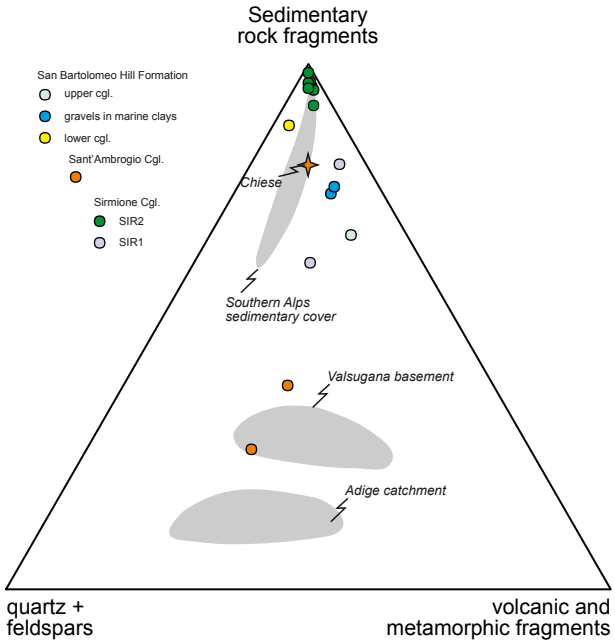

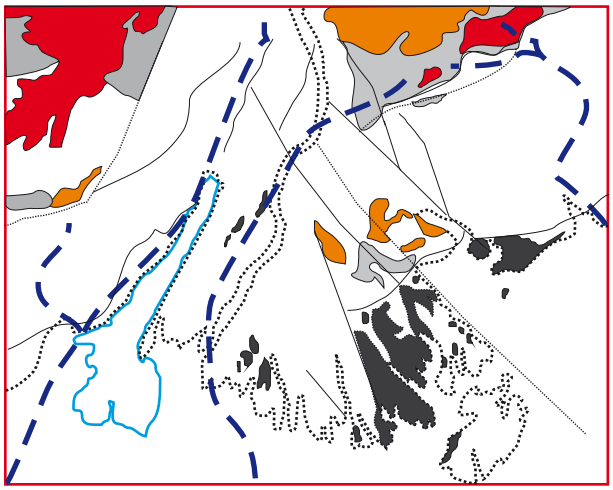

Pliocene

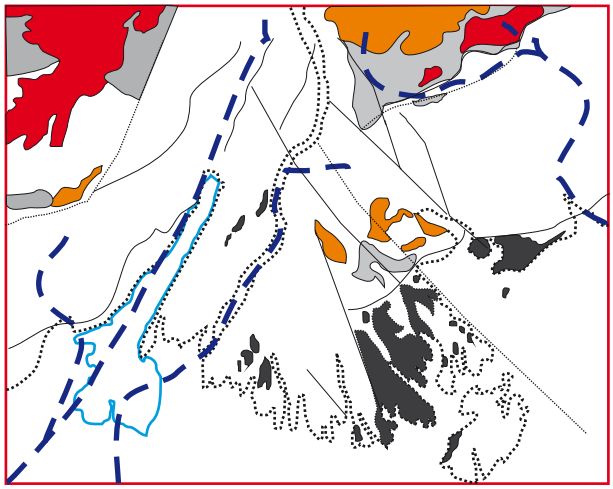

Early Pleistocene

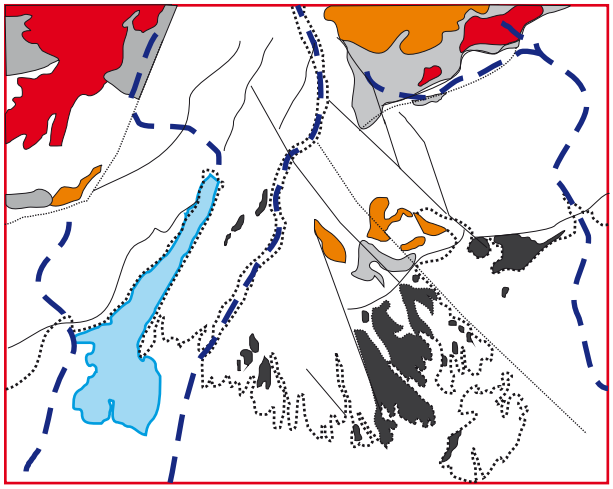

Middle Pleistocene

Figure 9

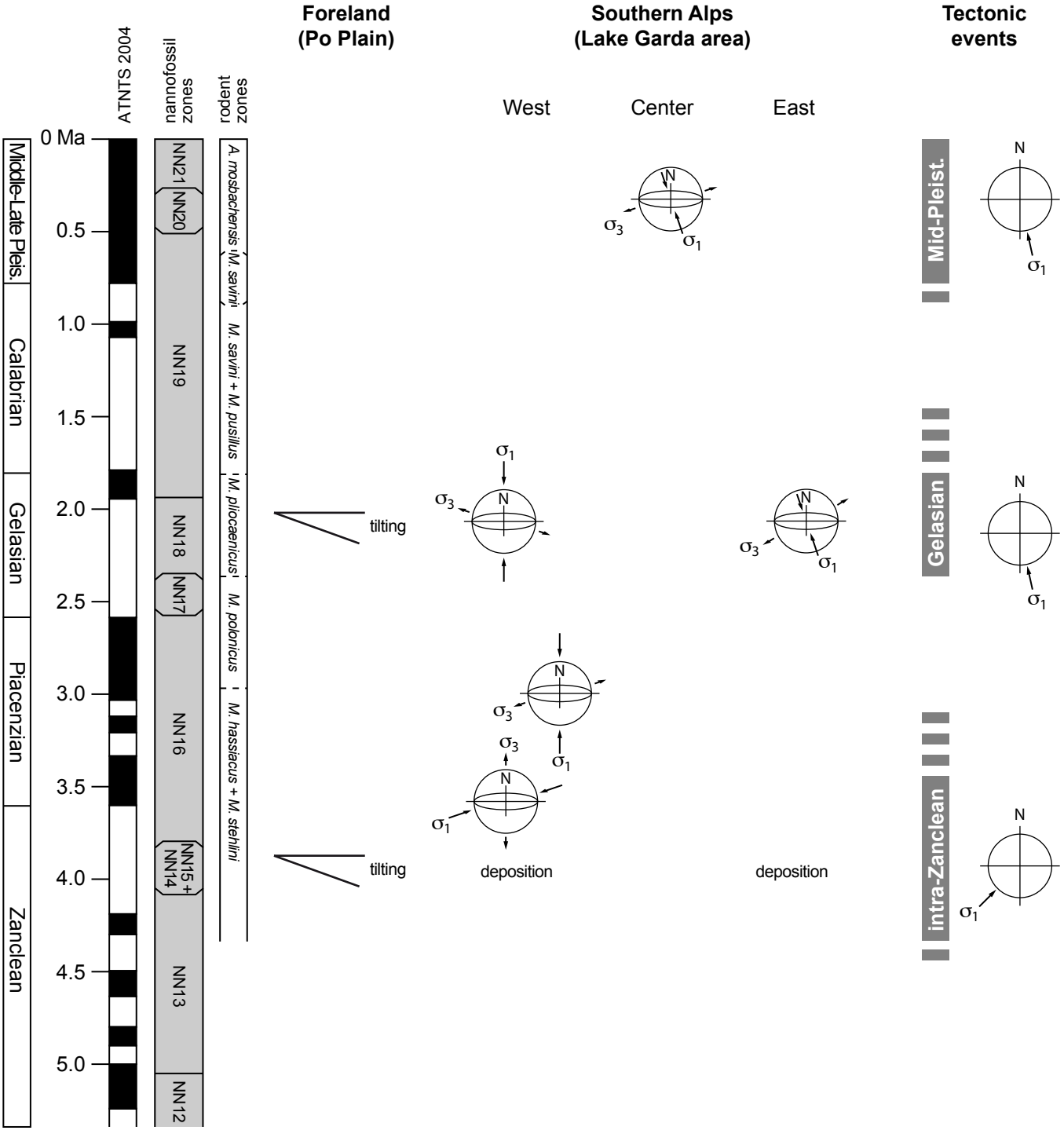
Foreland
(Po Plain)
Southern Alps
(Lake Garda area)
Tectonic
events
West
Center
East
ATNTS 2004
nannofossil
zones
rodent
zones
0 Ma
0.5
1.0
1.5
2.0
2.5
3.0
3.5
4.0
4.5
5.0
Middle-Late Pleis.
Calabrian
Gelasian
Piacenzian
Zanclean
NN21
NN20
NN19
NN18
NN17
NN16
NN15 + NN14
NN13
NN12
A. mosbachensis
M. savini
M. savini + M. pusillus
M. pliocaenicus
M. polonicus
M. hassiacus + M. stehlini
tilting
tilting
deposition
deposition
Mid-Pleist.
Gelasian
intra-Zanclean
N
σ1
σ3

Figure 10

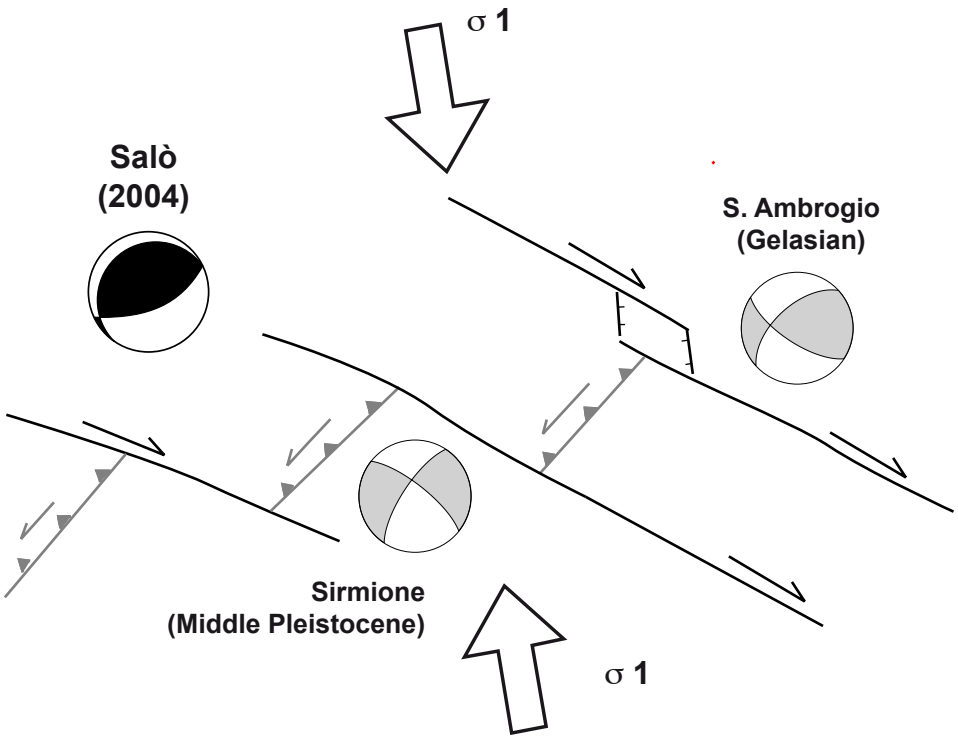
σ 1
Salò
(2004)
S. Ambrogio
(Gelasian)
Sirmione
(Middle Pleistocene)
σ 1

Figura 11

TABLE 1. DETRITAL MODES OF PLIOCENE–PLEISTOCENE SANDSTONES FROM THE LAKE GARDA AREA

	San Bartolomeo Hill Formation				Montecio Conglomerate			Sirmione Conglomerate								
	SB1	SB2		SB3				SIR1			SIR2					
Sample:	SB18	SB20	SB21	SB24	SA1	SA2	SA3	SIR13	SIR11	SIR17	SIR1	SIR2	SIR5	SIR6	SIR7	SIR8
Q	2.2	5.6	5.2	6.0	7.1	45.1	30.8	3.1	4.4	17.7	1.6	1.6	1.3	1.5	0.9	2.2
Kf	0.3	3.1	2.4	2.7	0.9	1.0	2.8			0.6				0.3		
P							0.3			0.3						
Lvf	7.6	10.9	10.5	17.6	5.6	5.9	11.2	4.0	13.2	8.2	1.9	3.2	1.3	1.5	0.3	1.6
Lvi			0.3				0.6			0.3						
Lvb					0.6	0.7	0.3									
Lvp								0.9	0.8	1.8						
Lcc	25.1	19.7	18.4	27.1	77.2	16.8	34.7	62.7	18.7	10.8	51.5	55.5	49.4	48.0	49.6	47.8
Lcd	57.3	49.7	47.9	27.4	0.9	2.4	0.8	14.3	61.0	45.9	23.2	25.6	32.1	30.7	35.9	35.1
Lp	6.0	6.0	10.2	14.6	1.8	6.6	2.2	3.1	1.4	4.0	6.7	2.6	1.6	6.4	3.7	4.8
Lch	0.6				2.1	0.7	1.1	11.8		1.3	14.5	11.4	13.8	11.4	9.4	7.8
Lms	0.9	4.4	2.7	4.6	3.5	19.6	14.8		0.5	7.9	0.6		0.5	0.3	0.3	0.6
Lmi		0.6	2.4		0.3	1.0	0.3			1.1						

Note: Q—quartz; Kf—K-feldspar; P—plagioclase; Lvf—felsic volcanic and subvolcanic lithic fragments; Lvi—intermediate volcanic and subvolcanic lithic fragments; Lvb—basic volcanic and subvolcanic lithic fragments; Lvp—plutonic lithic fragments; Lcc—limestone grains; Lcd—dolostone grains; Lp—shale, siltstone lithic fragments; Lch—chert grains; Lms—low-grade metamorphic lithic fragments; Lmi—medium-grade metamorphic lithic fragments.

TABLE 2. NANNOFOSSIL DISTRIBUTION CHART FOR THE SAN BARTOLOMEO HILL FORMATION AND THE BEDROCK OF THE SIRMIONE PENINSULA ("SCAGLIA" FACIES)

	San Bartolomeo Hill Formation, SB2 member							
Sample:	SB5	SB6	SB7	SB8	SB9	SB10	SB11	SB12
Preservation:	M	P	M	M	M	M	P	M
Abundance:	F	R	R	R	R	R	R	R
Braarudosphaera bigelowii					1			
Calcidiscus leptoporus	2		1	1	1	1		1
Coccolithus pelagicus	6	1	5	4	7	8	2	4
Helicosphaera carteri	5	1	2	1	6	7	1	9
Helicosphaera sellii	2		1		1	1		1
Pseudoemiliania lacunosa					2	2	1	2
Reticulofenestra minuta group	16	3	11	12	10	18	5	6
Reticulofenestra pseudoumbilica	33	6	19	22	10	13	5	3
Pseudoemiliana ovata	2		1	1	1	1		
Calcidiscus macintyrei	1			1				1
Discoaster spp.	1			1				2
Sphenolithus abies	5	1		2		3	1	2
Umbilicosphaera jafari	1			1				
Discoaster variabilis						1		
Reworked Cretaceous	21	4	19		31	44	5	31
Reworked Paleogene			4		11	12	2	8
Calcareous nannofossil zone (Martini, 1971)	NN14	NN14	NN14	NN14	NN15	NN15	NN15	NN15

	Sirmione peninsula bedrock (Scaglia)				
Sample:	SCA6	SCA4	SCA1	SCA2	SCA3
Preservation:	M	P	P	P	M
Abundance:	F	R	R	R	F
Arkhangelskiella cymbiformis	1	1	1	1	1
Broinsonia parca	1	1	1		1
Chiastozygus litterarius	1	1	1		1
Cretarhabdus conicus	1				1
Cribrosphaerella ehrenbergii	3	1	2	1	1
Cylindralithus spp.	1				
Eiffellithus eximius	1	2	1	1	1
Eiffellithus turriseiffelii	1	1	1	1	1
Gartnerago segmentatum	1		1		1
Microrhabdulus decoratus	1				
Micula staurophora	1	1	1	1	1
Prediscosphaera cretacea	1	1	1	1	1
Prediscosphaera spinosa	1	1		1	
Quadrum gartneri	1	1	1	1	1
Reinhardtites anthophorus	1	1		1	1
Retecapsa crenulata	3	1	1		1
Retecapsa schizobrachiata	1	1			
Staurolithites crux	1				
Tegumentum stradneri	1		1		1
Tranolithus orionatus	1	1	1	1	1
Watznaueria barnesae	5	1	1	3	4
Zeugrhabdotus elegans	1	1			
Zeugrhabdotus embergeri	1	1			1
Zeugrhabdotus erectus	1				
Gartnerago obliquum		1			
Hexalithus gardetiae		1	1		1
Kamptnerius magnificus		1			1
Lucianorhabdus cayeuxii					1
Reinhardtites levis	1		1	1	1
Zeugrhabdotus diplogrammus					1
Quadrum trifidum	1			1	
Calcareous nannofossil zone (Sissingh, 1977)	CC22c	CC22c	CC22c	CC22c	CC22c

Note: Abundance is expressed as F (frequent) and R (rare), preservation as M (moderate) and P (poor).

[[Please double check spelling of all Latin names.]]

TABLE 3. POLLEN DATA (RAW COUNTS AND PERCENTAGE VALUES) FOR THE SAN BARTOLOMEO HILL FORMATION AND THE SIRMIONE CONGLOMERATE

	Sirmione						San Bartolomeo	
	SI 24		**SI 25**		SI 26		SB 22	
	grains	pollen %	grains	pollen %	grains	pollen %	grains	pollen %
Gymnosperms								
Pinus sylvestris/mugo	211	52	266	65.8	62	58.5		
Pinus cembra	17	4.2	10	2.5	9	8.5		
Pinus diploxylon type							41	20.3
Pinus haploxylon type							5	2.5
Picea	54	13.3	35	8.7	24	22.6	24	11.9
Abies			3	0.7	4	3.8	19	9.4
Cathaya							75	37.1
Tsuga							24	11.9
Sciadopitys							1	+
Ephedra distachya type	76	18.7	9	2.2				
Ephedra fragilis type	7	1.7						
Total gymnosperms	365	89.9	323	80	99	93.4	189	93.6
Woody angiosperms								
Alnus glutinosa type			1	+	1	+	3	1.5
Betula			4	1			1	+
Carpinus orientalis							1	+
Ericaceae							1	+
Fagus							2	1
Hippophae	2	0.5	12	3				
Juglans							1	+
Deciduous *Quercus*							1	+
Tilia	1	+						
Total woody angiosperms	3	0.7	17	4.2	1	+	10	5
Upland herbs								
Gramineae	8	2	21	5.2				
Anthemis type			1	+				
Centaurea scabiosa	4	1	3	0.7				
Artemisia	13	3.2	20	5	2	1.9	1	+
Cichorioideae	9	2.2	15	3.7	4	3.8	1	+
Chenopodiaceae	1	0.2	2	0.5				
Helianthemum	5	1.2						
Caryophyllaceae			1	+				
Umbelliferae			1	+				
Polygonum viviparum	1	+						
Cruciferae							1	+
Total upland herbs	41	10.1	64	15.8	6	5.7	3	1.5
Aquatic and wetlands								
Cyperaceae	2	0.5	1	+				
Epilobium	3	0.7	4	1				
Thalictrum								
Total aquatic and wetlands	5	1.2	4	1				
Reworked palynomorphs								
Picea	22	5.4	9	2.2	13	12.3		
Pinus	312	76.8	111	27.5	164	154.7		
Abies	1	+			2	1.9		
cf *Cathaya*	6	1.5	1	+	7	6.6		
Cedrus					1	+		
Classopollis	5	1.2	1	+	2	1.9		
Unidentified 4-porate	1	+						
Unidentified 3-porate			1	+	1	+		
Taxodiaceae					1	+		
Cf. *Corylus*					1	+		
Carbonized *Pinus*					3	2.8		
3-porate cf. *Carya*	1	+						
Total reworked palynomorphs	348	85.7	123	30.4	195	184		
Nonpollen palynomorphs (sensu van Geel, 1978 [[Not in Refs list.]])								
Glomus					11	10.4		
Pteridophytes								
Monolete spores							7	3.5
Pteris							3	1.5
Marine microfossils								
Cysts of Dinoflagellata	6	1.5			8	7.5	1	+

Pollen sum (aquatic and wetlands excluded)	406	404	106	202
Pollen sum (aquatic and wetlands included)	411	408	106	202
Total number of taxa	17	18	7	17
Pollen concentration (grains/cm^3)	14315	11232	555	1794
Charcoal concentration (part./cm^3)	723	413	185	35
Reworked palynomorph concentration (grains/cm^3)	11975	3386	2371	/

Note: Pollen percentages are based on a pollen sum consisting of trees, shrubs, and upland herbs. Pollens of aquatic/wetland species, reworked, and nonpollen palynomorphs, Pteridophyte spores, and marine microfossils are excluded from the main pollen sum.

[[Please double check spelling of all Latin names.]]